日本原子力研究開発機構

Study on In-core Behavior of PWR Fuel under Power Transient

-Influence of Waterside Corrosion-

Kazuaki YANAGISAWA

Policy Planning and Administration Department

JAEA-Review

Study on In-core Behavior of PWR Fuel under Power Transient
-Influence of Waterside Corrosion-

Kazuaki YANAGISAWA

Policy Planning and Administration Department, Japan Atomic Energy Agency
Watanuki-machi, Takasaki-shi, Gunma-ken

The integrity of the PWR fuel under the power transient was studied taking into consideration of the waterside corrosion and the rod pressurization as test variables. Concluding remarks are as follows;

(1) For the pressurized PWR fuel up to 3.1-3.6MPa, the waterside corrosion had no effect on the fuel failure, occurred by the ballooned/rupture mechanism. The failure threshold was the same as that observed in the standard fuel.

(2) For the unpressurized PWR fuel, the waterside corrosion had a significant effect to preventing the fuel from the failure, occurred by the melt/brittle mechanism. The corroded film tended to minimize the temperature gradient across the cladding. It also worked to prevent the additional oxide formation, where the hoop stress raised during the quench was tended to reduce. As a result, the failure threshold of the corroded fuel was higher than that of the standard fuel.

(3) The use of the ZrO_2 fuel under the unpressurized condition revealed that the magnitude of PCST, ΔT were suppressed and the time to quench was shortened when they compared with those of the standard fuel. For example, PCST was 1,748 deg. C for the standard fuel but 1,285 deg. C for the corroded fuel (80μ m) at the energy deposition of 256cal/g・fuel. The PCST by 463 deg. C was suppressed to prevent from the failure.

(4) For the axial PCMI, the peak axial strain for the pressurized fuel increased with the increase of the ZrO_2 film; the maximum was 4% for the 40μ m fuel. Hence, at the outermost rim the ZrO_2 film suppressed the cladding to balloon. By contrast, the peak axial strain for the unpressurized fuel was not exceeded 1% irrespective to the ZrO_2 film. This was due to the strong axial restriction occurred by the rapid radial movement of the hot fuel. For the radial PCMI, the residual diametral strain remained little in the fuel rod with ZrO_2 film.

出力過渡を受けた PWR 燃料の炉内ふるまいに関する研究

-水側腐食の影響-

日本原子力研究開発機構経営企画部

栁澤　和章

出力過渡を受けた PWR 燃料の健全性につき、水側腐食の程度および燃料棒の加圧量を実験因子として研究した。得られた結論は以下のとおりである。

（1）3.1-3.6MPa まで加圧した加圧 PWR 燃料は膨れ/破裂メカニズムで破損したが、この破損メカニズムに水側腐食の影響は無かった。破損しきい値は標準燃料で観察されたものと同じであった。

（2）非加圧 PWR 燃料は被覆管の溶融/脆化メカニズムで破損したが、この破損メカニズムに水側腐食は大きな影響を及ぼし破損回避の方向に作用した。腐食膜は被覆管に発生した温度勾配を最小化し、被覆外面にさらなる腐食膜が生成するのを阻止し、クエンチ時に発生する円周応力を低下させた。その結果、腐食膜付 PWR 燃料の破損しきい値は標準燃料で観察されたものより高かった。

（3）ZrO_2 酸化膜付 PWR 燃料を非加圧状態で使用すると、被覆管最高温度（PCST）やクエンチ温度幅（ΔT）が低く抑えられ、急冷時間が短くなる事が標準燃料との比較で明らかになった。例えば、発熱量 256cal/g・fuel.において、標準燃料で 1,748 度だった PCST が 80μm酸化膜付燃料棒で 1,285 度と、463 度も下がった。

（4）軸方向のペレット-被覆管機械的相互作用（PCMI）についてみると、加圧燃料の軸最大歪は ZrO_2 酸化膜厚の増加と共に増加し、40μmで最大 4%となった。燃料棒の外縁において ZrO_2 酸化膜は被覆管が膨れるのを阻止する働きがある。一方、非加圧燃料の軸最大歪は ZrO_2 酸化膜厚とは無関係に 1％を越えなかった。高温化した燃料の径方向膨張によるギャップの喪失により、軸方向の動きに大きな抑圧が掛かったためである。径方向の PCMI についてみると、残留径歪はどの燃料棒でも小さかった。

高崎量子応用研究所(駐在)：〒370-1292　群馬県高崎市綿貫町 1233

This is a blank page.

Contents

目次

1. INTRODUCTION

In the field of the safety research on a light water reactor (LWR) fuel, a reactivity initiated accident (RIA) is one of the important phenomena, especially for the data as the licensing. Since 1975, the experimental study on RIA was done in the Nuclear Safety Research Reactor (NSRR) belonged to the Japan Atomic Energy Agency (the former Japan Atomic Energy Research Institute; JAERI). In the pulse irradiation test, a 14x14 pressurized water reactor (PWR) type segmented fuel having an active fuel column length of about 135mm and a fuel enrichment (^{235}U) of 10 wt% was defined as the standard fuel. Note that they were fresh fuels, that is, zero burn-up before pulse.

In most cases, the fuel rod was pulse irradiated with a filler gas as much as 0.1MPa, where the gas composition was 100% helium. This is because the pressure of the coolant (H_2O) in an irradiation capsule was 0.1MPa. In several cases, the NSRR test fuel was intentionally pressurized to 3.2MPa, which was the same situation to the fuel rod used in the commercial power reactor.

A failure mechanism revealed for the unpressurized standard fuel was the melt/brittle of the zircaloy-4 cladding and the ballooning/rupture for the pressurized fuel. A failure threshold for the former was 260cal/g・fuel in the deposited energy and that for the latter was 110cal/g・fuel in the enthalpy. These observations were quoted to the Japanese Licensing Guideline for RIA and the past NSRR report [19].

With respect to the fuel characterization, the NSRR standard fuel has partly different point from the practical PWR fuel. One marked point is that the NSRR standard fuel had no waterside corrosion, that is, a thin film made of ZrO_2 on the external surface of the zircay-4 cladding. Taking this situation into consideration, the author intended to carry out the RIA test by the fresh PWR fuels having ZrO_2. As the second parameter, the rod internal pressure (0.1MPa and 3.2MPa) was chosen..

Preliminary studies to understand the failure threshold for an unpressurized fuel with /without ZrO_2 and those for a pressurized fuel with/without ZrO_2 were made. Results obtained form the former [20] and those obtained from the latter [21-23] were reported separately. The present paper is mainly to study the failure mechanism basing on in-core performance data; those were not discussed in the previous studies.

2. EXPERIMENTAL METHOD

2.1 Test parameters

(1) Waterside corrosion

According to PIE data [1-8], the waterside corrosion or the external corrosion of the PWR type fuel rod as a function of burn-up is burn-up dependent as shown in **Fig.1.** It is clear that the ZrO_2 film was increased with an increase of burn-up up to 60MWd.kgU. From the viewpoint of the licensing, this phenomenon is important because the increase of
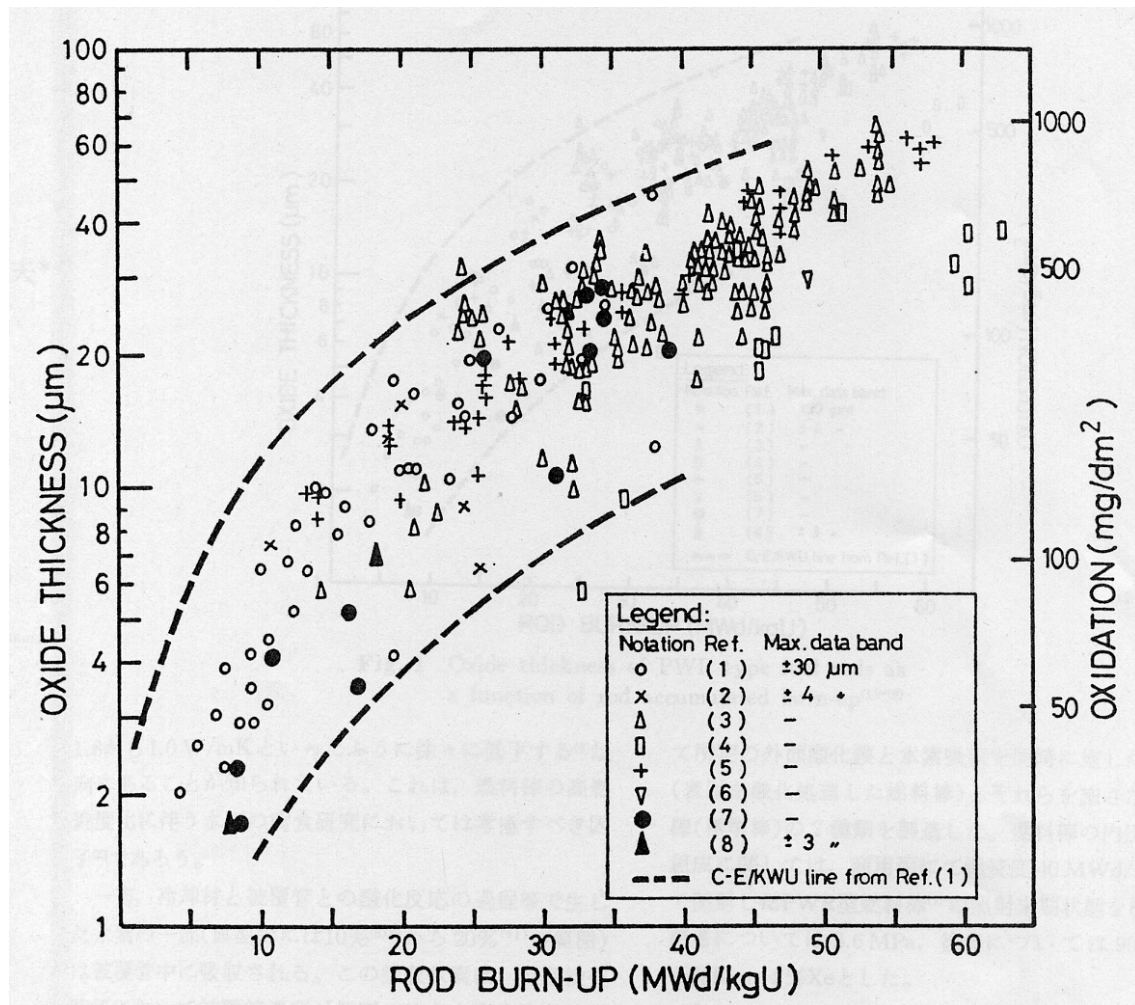

Fig.1 Oxide thickness of the PWR type fuel rods as a function of rod accumulated burn-up [1-8]

ZrO_2 film will be degraded the heat conductance of the cladding, for example, from

1.8W/mK to 1.0W/mK. The degradation makes the PWR fuel temperature hot [9-10], and should enhance the fission gas release (FGR). The generated FGR was strongly linked the increase of the rod internal pressure at the gas gap and plenum. It should be mentioned that in the licensing criteria in Japan, the rod internal pressure is prohibited strictly to excess the coolant pressure at the end-of life (EOL).

During the formation of ZrO_2 film, amounts of hydrogen (H_2) will be generated as the result of the reaction between the H_2O coolant and the zircaloy-4 cladding. A part of the generated hydrogen, namely about 10% [5, 10] to 20% [11] of the total will be picked-up into the cladding and started to make the cladding brittle during the subsequent irradiation period.

As shown in **Table 1**, the author selected nine different kinds of ZrO_2; they were estimated by the upper C-E/KWU line in the Fig.1.   Amounts of picked-up hydrogen were also taken into consideration. The author expects that experimental results can be used as a supplemental database for the existing RIA Licensing Guideline [12].

Table 1 Test parameters

Characteristics	17×17 PWR, pressurized group					14×14 PWR, unpressurized group				
Fuel Rod Type	ZrO_2 Corroded				Reference (Standard)	ZrO_2 Corroded				Reference (Standard)
Fuel Rod No.	P13, P14	P15, P16	P17, P18	P19, P20	P7, P8, P9, P24, P2, P5	J0, J1	J2, J3	J4, J5	J6, J7	J23, J24, J25, J26
Oxide Thickness (μm)	10	20	30	40	0	50	60	70	80	0
Absorbed Hydrogen (ppm)	50	120	140	70(a)	0	91	133	183	344	0
Fill gas pressure(MPa, 20deg.C)	3.0-3.6					0.1				
Fill gas composition (vol.%)	95%He+1%Kr+4%Xe(b)					100%He				

Note：(a) Absorbed hydrogen for P19 and P20 did not reach the targeted value due to the change of cladding inside condition after the oxidation
　　　(b)Fill gas compsition was decided by the PWR fuel rod irradiated to 40MWd/kgU, of which FGR was 0.6%.

(2) Rod internal pressure

With respect to the rod internal pressure and the gap gas composition, a PWR rod irradiated to 40MWd/kgU in the Japanese commercial power reactor was referred to the present study [7]. From the PIE of the fuel rod, it was revealed that the FGR was the 0.6%, the rod internal pressure the 3.6MPa and gas composition the 95%He+1%Kr+4%Xe. These referential values were directly applied to the case of the pressurized fuels as shown in the left half of Table1, that is, the columns from 2 to 6. Hereinafter the author denoted them as the "pressurized group".

At EOL of the PWR fuel, the difference between the PWR rod internal pressure and the coolant one is getting small in magnitude because of the creep-down, fuel swelling and FGR. The author found that such EOL condition is significantly resembled between the

NSRR standard fuel (the rod internal pressure is 0.1MPa) and the coolant pressure in the irradiation capsule (0.1MPa). This finding was directly applied to the case of the unpressurized fuels as shown in the right half of the Table1, that is, the columns from 7 to 11. The author denoted them as the "unpressurized group". The ZrO_2 film in the unpressurized group is thicker than that of the pressurized group. Common to the two cases, the referential fuels having no ZrO_2 were introduced as shown in the columns 6 and 11. They denoted here as the reference or standard fuels.

2.2 Fabrication of the test fuel rod

The test fuel rods were originally designed by the JAEA and fabricated by the Nuclear Development Corporation (NDC), Tokai, Japan.

(1) Oxidation of the cladding

According to Garzarolli et al[1], the oxide thickness was increased with a rate of 10μ m per 10MWd/kgU. The author prepared eight zircaoy-4 tubes and sealed both top and bottom end. Subsequently they were heated up to 450 deg. C in the oxidized atmosphere. Dismantled days for the pressurized group were 33, 64, 95 and 125 to get the external oxide of 10, 20, 30 and 40μ m. Those for the unpressurized group were 145, 175, 200 and 230 days to get the external oxide of 50, 60, 70 and 80 μ m. For the all cases, the author got the expected thickness of the oxides.

(2) Hydriding of the cladding

The author assumed that during the oxidation process about 10% of the generated amounts of the hydrogen were picked up into the cladding. After cutting the sealed ends of the autoclaved tubes, eight tubes were heated up to 400 deg. C in the reduced (H2 gas) atmosphere. Expected amounts of hydrogen for the pressurized group were 52, 104, 155 and 207ppm for the 10, 20, 30 and 40μ m autoclaved tubes. Practical values obtained were 50, 120, 140 and 70ppm. The 70ppm instead of 207ppm was happened without the clear reason. Expected amounts of hydrogen for the unpressurized group were 260, 310, 360 and 410ppm for the 50, 60, 70 and 80μ m autoclaved tubes. Practical values obtained were 91, 133, 183 and 344ppm. Practical values were of the order of 35%-80% of the expected amounts. The mechanism of the hydrogen puck-up occurred in the in-pile irradiation might be more complicated than that of the out-of-pile test.

With respect to the pressurized group, the left-hand side of **Photo.1** shows the test tube having the oxide thickness by 20μ m and the picked-up hydrogen by 120ppm. The right-hand side shows the PIE photograph of the irradiated PWR fuel rod up to

34MWd/kgU, where oxide thickness was about 20μm but the amounts of the picked-up hydrogen was unknown[8]. The oxide film obtained from the out-of-pile condition seems to be rather coarse than that of the in-pile one, and the picked-up hydrogen distributed more uniformly than in-core one.

With respect to the unpressurized group, two representative metallographic pictures are shown in **Photo.2.** At moment the author does not have PIE data comparable with those two. X-ray inspection to those eight tubes revealed no anomalies at all.
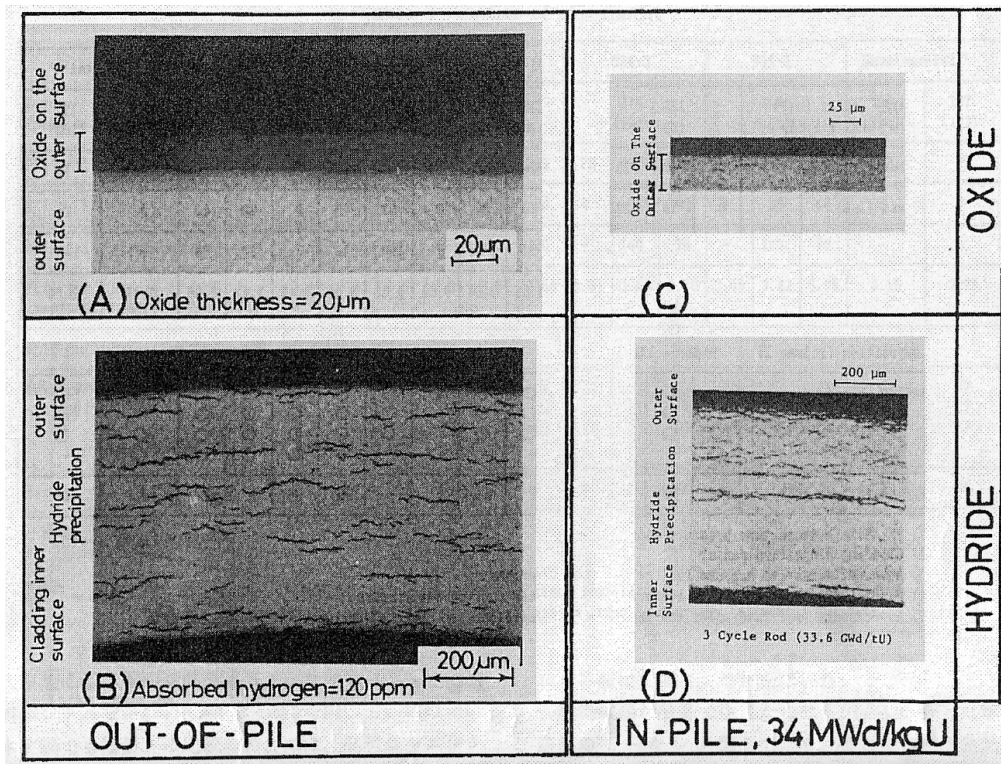

Photo.1 Two pictures shown in the left-hand side were metallographic pictures for oxide film by 20μm (A) and picked-up hydrogen by 120ppm, Two pictures shown in the right-hand side were from PIE of the PWR fuel rod burned to 34MWd/kgU[8], where the oxide film was about 20μm(C) but amounts of picked-up hydrogen was unknown. (D). All data are for pressurized fuels.
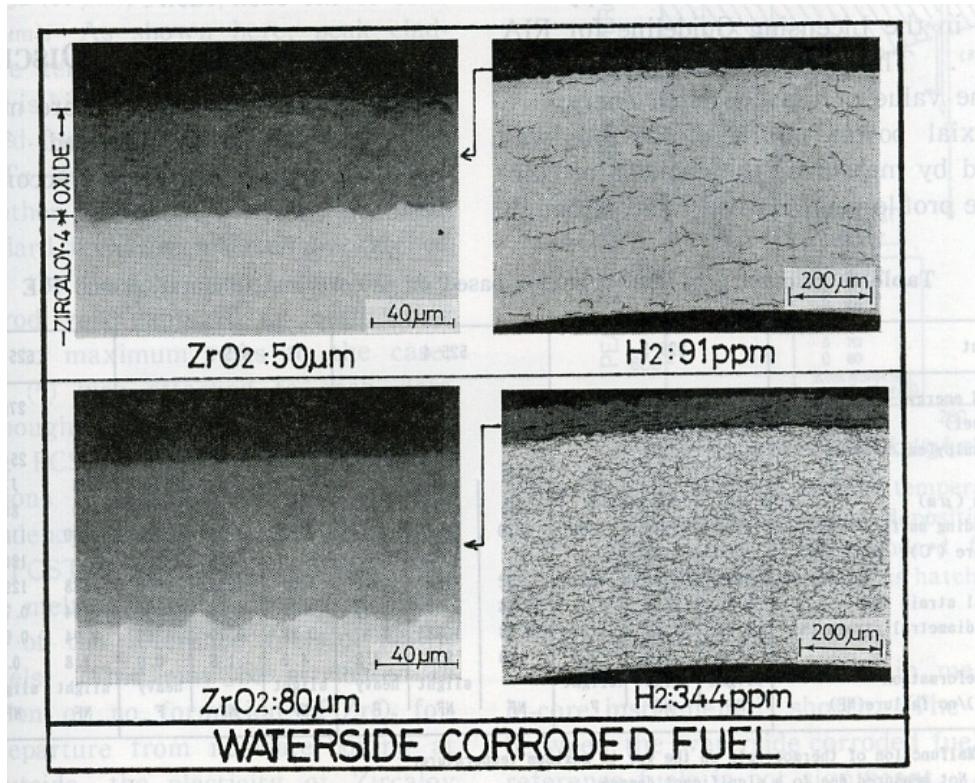
Photo.2 Representative cross section of the waterside corroded cladding tubes; (Top) 50 μ mZrO$_2$ and 91ppm hydrogen and (Bottom) 80 μ mZrO$_2$ and 344ppm hydrogen. All data are for unpressurized fuels.

(3) Fuel rod

The enrichment of the UO$_2$ fuel was 10wt% for the active column length and 3.4 or 0.26 wt% for the end of the active column. All pellets had about 95% of the theoretical density (T. D.) and grain size diameter determined by the two dimensional intercept method was about 8-10 μ m. As-fabricated characteristics of the fuel rods were summarized in the **Table 2**.

The longitudinal cross section of the test fuel rod provided for the pressurized group is shown in **Fig.2**.

Fig.2 Longitudinal cross section of the test fuel rod provided for the pressurized group

Table 2 As-fabricated fuel characteristics used

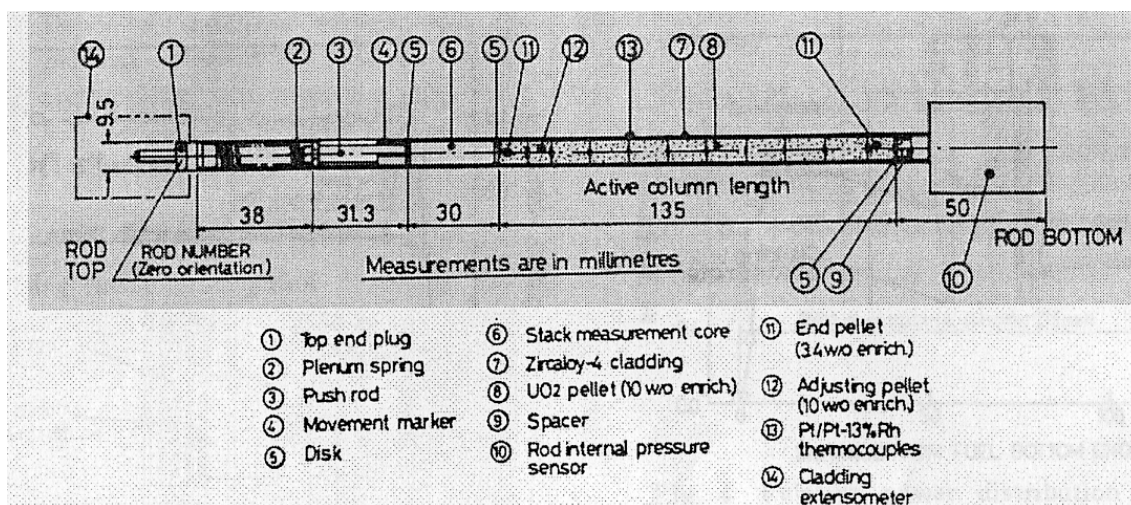| Fuel Rod Type		Pressurized group					Unpressurized group				
Fuel Rod No.		P13/P14	P15/P16	P17/P18	P19/P20	P7, P8, P9, P24, P2, P5	J0/J1	J2/J3	J4/J5	J6/J7	J23, J24, J25, J26
1. Fuel pellet		Sintered and ground UO₂ pellets					Sintered and ground UO₂ pellets				
	Enrichment (wt %)	10.0(Active column), 3.4(end pellet)					10.0(Active), 3.4(end)				10.0(Active), 0.27(end)
	Density (%TD)	95.10					95.44				94.77
	Outer diameter (mm)	8.19					9.29				
	Length (mm)	13.5					15.2				10.0
	End form	Double dishing					Double dishing				Double chamfer
		(5.97mm O. D.×0.3mm depth)					(6.7mm O. D.×0.3mm depth)				(0.35mm width×0.14mm height)
	Grain size (μm)	8.0					9.6				9.4
2. Cladding		Stress relieved zircaloy-4					Stress relieved zircaloy-4				(Zr+1.43%Sn+0.20%Fe+0.11%Cr)
	Outer diameter (mm)	9.50					10.72				
	Inner diameter (mm)	8.36					9.48				
	Wall thickness (mm)	0.57					0.62				
	Oxide Thickness (μm)	10	20	30	40	0	50	60	70	80	0
	Absorbed Hydrogen (ppm)	50	120	140	70(a)	0	91	133	183	344	0
3. Fuel rod		17×17 type PWR fuel rod					14×14 type PWR fuel rod				
	Diametral gap (mm)	0.17					0.19				
	Fill gas pressure (MPa, 20deg.C)	3.0-3.6					0.1				
	Fill gas composition (vol.%)	95%He+1%Kr+4%Xe(b)					100%He				
	Plenum volume (c.c.)	2.7					2.6				
	Fuel column (mm)	116mm (10.0wt%)+19mm (3.4wt%)					113mm (10.0wt%)+23mm (3.4wt%)				115mm(10.0wt%)+20mm(0.27wt%)

Note : (a) Absorbed hydrogen for P19/P20 did not reach the target value due to the change of cladding inside condition after the oxidation.

(b) Fill gas composition was decided that the fuel rods was 0.6% FGR at the burn-up of 40MWd/kgU.

2.3 Fuel assemblies, irradiation capsule and instrumentation

Three test fuel rods wee arranged in a triplet rod configuration. They were located 120deg. C apart in a circle having 18mm radius. This arrangement can minimize the radial power distortion and avoids thermal interaction between the loaded rods. The midpoint of the active column of the test fuel rods was coincided with NSRR core midplane. As shown in previous Fig.2, a cladding extensometer (EC) to measure the rod axial deformation was attached to the top of the each fuel rod. A Pt/Pt-13%Rh type thermocouple (T/C) to measure the cladding temperature was directly spot welded after abrading oxides in a limited small area. Their locations were middle of the active fuel column and ±33mm apart from the middle point. A strain gauge type pressure sensor was attached to the rod bottom to monitor the change of the rod internal gas pressure. Lastly, the movement marker made of the zirconium ring was set to the just top part of the fuel column to monitor the maximum movement of the fuel column. The moved distance was confirmed by the X-ray at PIE.

Three fuel rods were assembled to the supporting jig together with the electric wires and loaded into the irradiation capsule as shown in the **Fig. 3**. The test fuel rods were immersed in the stagnant water at room temperature (usually about 20 deg. C) and atmospheric pressure inside a sealed irradiation capsule.
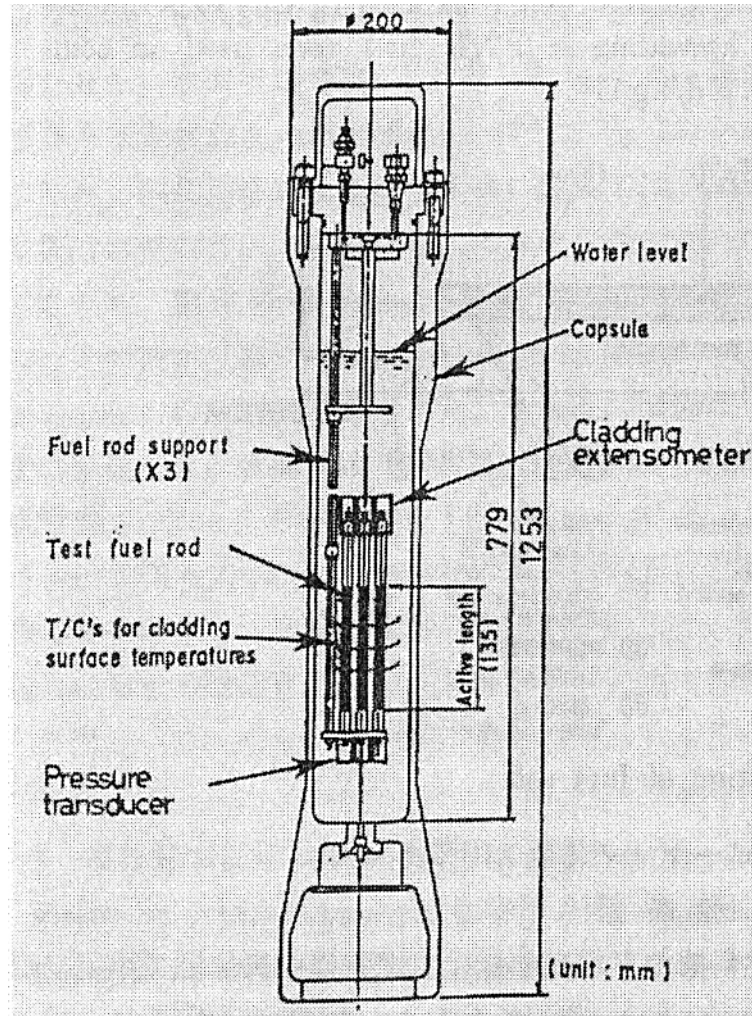
Fig.3 Irradiation capsule for the triplet rod configuration and attached in-core instrumentation

2.4 In-core pulse irradiation and pulse history

As shown in **Table 3**, the pressurized group in a triplet configuration was pulsed in the test series of 525-1, 525-2, 524-3 and 524-4 with a different magnitude of the deposited energy. Two standard rods, P2 and P5 were separately pulsed in single rod configuration. Meanwhile, the unpressurized group in a triplet configuration was pulsed in the test series from 525-3 to 525-6. Due to the limited space in the irradiation capsule, in-core instruments were assigned to each test fuel rod.

The integral value of the reactor power P (MW・s) was used to estimate the deposited energy Eg (cal/g・fuel) in each test fuel rod. Hence, $Eg=Kg \times P$, where the power

conversion ratio *Kg* (cal/g・fuel per MW・s) was determined through the fuel burn-up analysis taking the radial and axial power skew into consideration [13]. The error band of this analysis was within ±5%. Because the licensing guideline for RIA uses not only the deposited energy but also the radially averaged fuel enthalpy, the author concerted the deposited value into the enthalpy [14] for the reader's convenience. The following discussion however will mostly present the value with the deposited energy.

The axial power profile of the tested rods was determined by the use of nuclides ^{95}Zr-^{95}Nb. As shown in **Fig.4**, the profile was relatively flat, although the locally sharp peaks with about 30% for the reference fuels and with about 6% for the bottom end of the ZrO$_2$ fuels were observed. In fact, many tested fuels were defected at the bottom end.
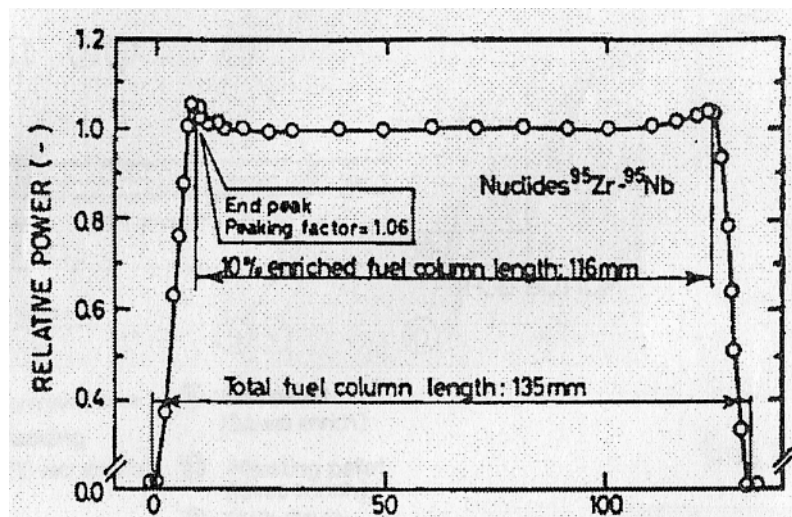

Fig.4 Relative power distribution of the test fuel rod determined by the axial gamma scanning

Table 3 Test matrix and instrumentations attached to the individual fuel rods

Pressurized group

Experiment.	525-1			525-2			524-3			524-4			Supplemental	
Deposited Energy (cal/g・fuel)	129			158			174			154			154	137
Enthalpy (cal/g・fuel)	95			125			142			121			121	103
Fuel rod	P7	P13	P15	P8	P14	P16	P9	P17	P19	P24	P18	P20	P2	P5
Oxide Thickness (μm)	0	10	20	0	10	20	0	30	40	0	30	40	0	0
Absorbed Hydrogen(ppm)	-	50	120	-	50	120	-	140	70	-	140	70	-	-
Fill gas pressure at 20deg.C	3.55	3.47	3.52	3.55	3.51	3.54	3.51	3.58	3.30	3.45	3.42	3.06	3.16	3.26
Fill gas composition (Vol.%)	95%He+1%Kr+4%Xe													
Instrumentation Equipped PF(a)	O	O	O	O	O	O	O	O	O	O	O	O	O	O
EC(b)	-	O	O	-	O	O	-	O	O	O	O	O	-	O
EF(c)	O	O	O	O	O	O	O	O	O	O	O	O	O	O
T/C(d)	O	-	-	O	-	-	O	-	-	O	O	O	O	-
Failure(F)/ No Failure (NF)	NF	NF	NF	NF	F	F	F	F	NF	NF	F	F	F	NF

Unpressurized group

Experiment	525-3			525-4			525-5			525-6		
Deposited Energy (cal/g・fuel)	256			256			262			279		
Enthalpy (cal/g・fuel)	232			232			238			254		
Fuel rod	J0	J4	J23	J2	J6	J25	J1	J5	J24	J3	J7	J26
Oxide Thickness (μm)	50	70	0	60	80	0	50	70	0	60	80	0
Absorbed Hydrogen(ppm)	91	183	0	133	344	0	91	183	0	133	344	0
Fill gas pressure at 20deg.C	0.10											
Fill gas composition (Vol.%)	100%He											
Instrumentation Equipped PF(a)	-	-	-	-	-	-	-	-	-	-	-	-
EC(b)	1	1	1	1	1	1	1	1	1	1	1	1
EF(c)	-	-	-	-	-	-	-	-	-	-	-	-
T/C(d)	2	3	2	2	3	2	2	3	2	2	3	2
Failure(F)/ No Failure (NF)	NF	F	F	NF	F	F	NF	NF	F	NF	NF	F

Note: (a)PF; Strain gauge type pressure sensor, (b) EC;Cladding elongation sensor, (c)EF;Movement marker, (d) T/C; Pt/Pt-13%Rh thermocouples

3. RESULTS AND DISCUSSION

The author summarized the data obtained from the in-core instrumentation and the PIE in the **Table 4**. The failure or no failure decision was made by PIE. According to these experimental data, the following discussions will be made

3.1 Failure threshold and failure mechanism

3.1.1 Pressurized group

For the case of the pressurized fuels, a data plot was followed the example shown in the Licensing Guideline for RIA [12]. **Fig. 5** is the result. The failure of the corroded (ZrO_2) fuels did not occur below the past NSRR experimental data line or below the acceptable design criteria of LWR. The test fuel rod P20 (40 μ m) failed at the enthalpy of 121 cal/g・fuel but the test fuel rod P19 (40 μ m) did not fail at the enthalpy of 142 cal/g・fuel. This discrepancy might be explained that the latter had a little pellet-cladding mechanical interaction (PCMI), accompanying with a little ballooning.
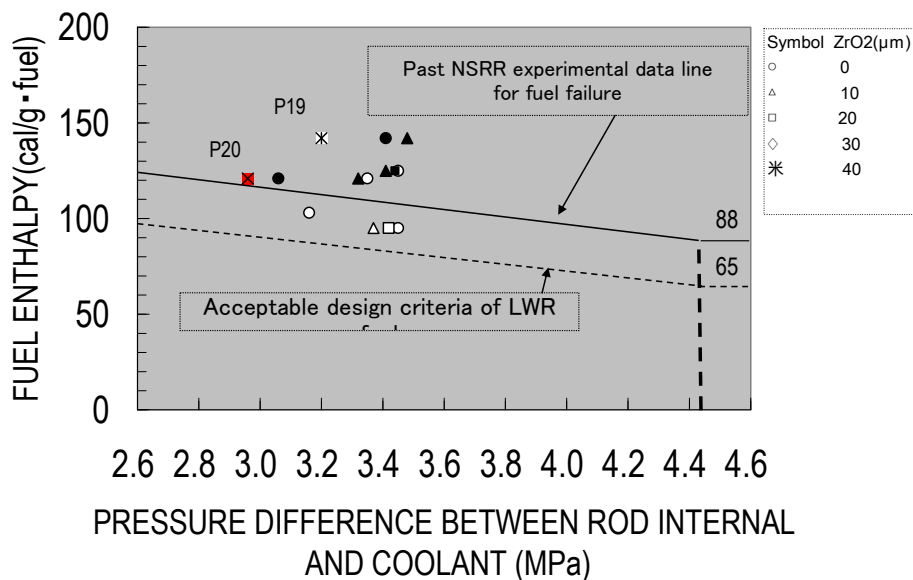

Fig.5 Deposited enthalpy of the tested fuel rod vs. pressure difference between the rod internal and the coolant, where the conventional LWR fuel design criteria under RIA standard fuels is also shown by the solid line (past NSRR experimental data line foe fuel failure) and dotted line (acceptable design criteria of LWR).

Table 4-1 Summary of the RIA tests carried out by the pressurized group; ZrO_2 varied from 10 to 40 μ m

Waterside Corroded Fuel (Pressurized 17x17 PWR)
Summary of fuel behavior

Pressurized group

	Parameter	P7	P13	P15	P8	P14	P16	P9	P17	P19	P24	P18	P20	P2	P5
1	Fuel Rod Type	17×17	17×17	17×17	17×17	17×17	17×17	17×17	17×17	17×17	17×17	17×17	17×17	17×17	17×17
2	Fuel rod	P7	P13	P15	P8	P14	P16	P9	P17	P19	P24	P18	P20	P2	P5
3	Experiment.	525-1	525-1	525-1	525-2	525-2	525-2	524-3	524-3	524-3	524-4	524-4	524-4	524-1	524-2
4	Oxide Thickness (μm)	-	10	20	-	10	20	-	30	40	-	30	40	-	-
5	Absorbed Hydrogen(ppm)	-	50	120	-	50	120	-	140	70	-	140	70	-	-
6	Fill Gas Composition (Vol.%) Mix: 95%He+1%Ke+4%Xe	Mix	Mix	Mix	Mix	Mix	Mix	Mix	Mix	Mix	Mix	Mix	Mix	Mix	Mix
7	Deposited Energy (cal/g·fuel)	129	129	129	158	158	158	174	174	174	154	154	154	154	137
8	Enthalpy (cal/g·fuel)	95	95	95	125	125	125	142	142	142	121	121	121	121	103
9	Fill gas pressure at 20deg.C, Po(MPa)	3.55	3.47	3.52	3.55	3.51	3.54	3.51	3.58	3.30	3.45	3.42	3.06	3.16	3.26
9*1	Pressure difference between rod internal and coolant (MPa)	3.45	3.37	3.42	3.45	3.41	3.44	3.41	3.48	3.2	3.35	3.32	2.96	3.06	3.16
9*2	Reached Peak Pressure :Pm (MPa)	3.96	3.88	3.95	4.01	3.94	3.96	3.98	4.06	3.82	3.93	3.96	3.51	3.58	3.63
9*3	Pressure Increase: Pm-Po (MPa)	0.409	0.413	0.425	0.46	0.43	0.42	0.47	0.48	0.52	0.48	0.54	0.45	0.42	0.37
9*4	Time at peak (s)	-	-	-	-	0.43	0.43	0.33	0.33	-	-	0.44	0.38	0.60	-
9*5	Time to failure (s)	-	-	-	-	0.43	0.87	0.49	0.87	-	-	0.66	0.55	0.99	-
10	PCST (deg.C) Max.	738	-	-	810	-	-	952	-	-	852	110	768	768	712
11	Time to quench (s)	0.11	-	-	0.13	-	-	0.27	-	-	0.16	-	0.11	0.51	0.49
12	ΔT(deg.C)	560	-	-	632	-	-	758	-	-	619	-	535	566	514
13	Coolant Temperature (deg.C) Before Pulse	16	16	16	-	-	-	20	20	20	-	-	-	20	12
14	After Pulse	25	25	25	-	-	-	31	31	31	-	-	-	33	18
15	Axial elongation Maximum (%)	-	-	-	-	2.50	2.71	-	3.93	3.67	-	0.15	0.66	-	-
15*1	Residual strain (%)	-0.04	0	0.06	-0.077	0.097	0.15	rupture	rupture	rupture	0.077	-0.096	-0.04	0.19	-
16	Residual diametral strain (%)	3.2	4.4	5.2	4.9	9.4	10.0	6.6	9.3	3.0	4.6	3.9	3.6	7.6	3.3
17	Maximum fuel column movement (%)	2.0	1.9	2.1	2.2	2.6	2.0	2.6	4.0	2.5	1.6	2.1	2.3	0.5	1.2
18	Fuel rod bow (mm)	None	None	None	None	None	None	None	None	None	None	None	None	Slight	None
19	Failure (F) / No failure (NF)	NF	NF	NF	NF	F	F	F	F	NF	NF	F(270°)	F(90°)	F	NF
20	PIE(f)	-	-	-	-	RB	RB	RB	RB	-	-	RB, SO	RB	RB	-

Note: (f)RB means rupture after ballooning at the rod bottom end, SO: Scaled off of the ZrO₂ film

Table 4-2 Summary of the RIA tests carried out by the unpressurized group; ZrO$_2$ varied from 50 to 80 μ m

Unpressurized group

		J23	J0	J4	J25	J2	J6	J24	J1	J5	J26	J3	J7
1	Fuel Rod Type	14x14	14x14	14x14	14x14	14x14	14x14	14x14	14x14	14x14	14x14	14x14	14x14
2	Fuel rod	J23	J0	J4	J25	J2	J6	J24	J1	J5	J26	J3	J7
3	Experiment.	525-3	525-3	525-3	525-4	525-4	525-4	525-5	525-5	525-5	525-6	525-6	525-6
4	Oxide Thickness (μm)	-	50	70	-	60	80	-	50	70	-	60	80
5	Absorbed Hydrogen(ppm)	-	91	183	-	133	344	-	91	183	-	133	344
6	Fill Gas Composition (Vol.%) Mix: 95%He+1%Ke+4%Xe	100%He	100%He	100%He	100%He	100%He	100%He	100%He	100%He	100%He	100%He	100%He	100%He
7	Deposited Energy (cal/g・fuel)	256	256	256	256	256	256	262	262	262	279	279	279
8	Enthalpy (cal/g・fuel)	232	232	232	232	232	232	238	238	238	254	254	254
9	Fill gas pressure at 20deg.C, Po(MPa)	0.1	0.1	0.1	0.1	0.1	0.1	0.1	0.1	0.1	0.1	0.1	0.1
9*1	Pressure difference between rod internal and coolant (MPa)												
9*2	Reached Peak Pressure :Pm (MPa)												
9*3	Pressure Increase: Pm-Po (MPa)												
9*4	Time at peak (s)												
9*5	Time to failure (s)												
10	PCST (deg.C) Max.	1800	1328	1490	1748	1320	1313	1166	1639	1269	1505	1800	1800
11	Time to quench (s)	-	4.2	2.6	7.1	3.7	2.2	-	3.8	2.5	-	2.5	2.5
12	ΔT(deg.C)	-	1228	1255±67	1648	1036	1073	-	1539	1098	-	1464	1302
13	Coolant Temperature (deg.C) Before Pulse	19	19	19	16	16	16	14	14	14	12	12	12
14	After Pulse	48	48	48	46	46	46	40	40	40	21	21	21
15	Axial elongation Maximum (%)	0.71	0.85	0.90	0.84	0.76	1.08	0.73	0.76	0.56	0.71	0.64	0.78
15*1	Residual strain (%)												
16	Residual diametral strain (%)	1.23	0.80	1.58	2.87	0.58	1.38	1.53	0.83	0.70	3.5	0.94	0.95
17	Maximum fuel column movement (%)												
18	Fuel rod bow (mm)	7.9	7.8	8.8	4.2	1.0	2.0	0.0	4.0	1.8	(a)	1.8	0.9
19	Failure (F) / No failure (NF)	F	NF	NF	F	NF	NF	F	NF	NF	F	NF	NF
20	PIE(f)	Melt/brittle	Slight WD	Slight WD	Melt/Brittle,7mm	SO at top	Slight WD	Broken	WD	SO at T/C	T/C SO	WD, SO	DC;SO

Note; (f) SO:ZrO$_2$ was partly scaled off from the surface, WD: Wrinkle deformation, DC: Discoloration

A failure mechanism for the pressurized group was examined in the PIE and found that all failure including the standard fuel occurred by the ballooning and rupture as shown in the **Photo.3**.
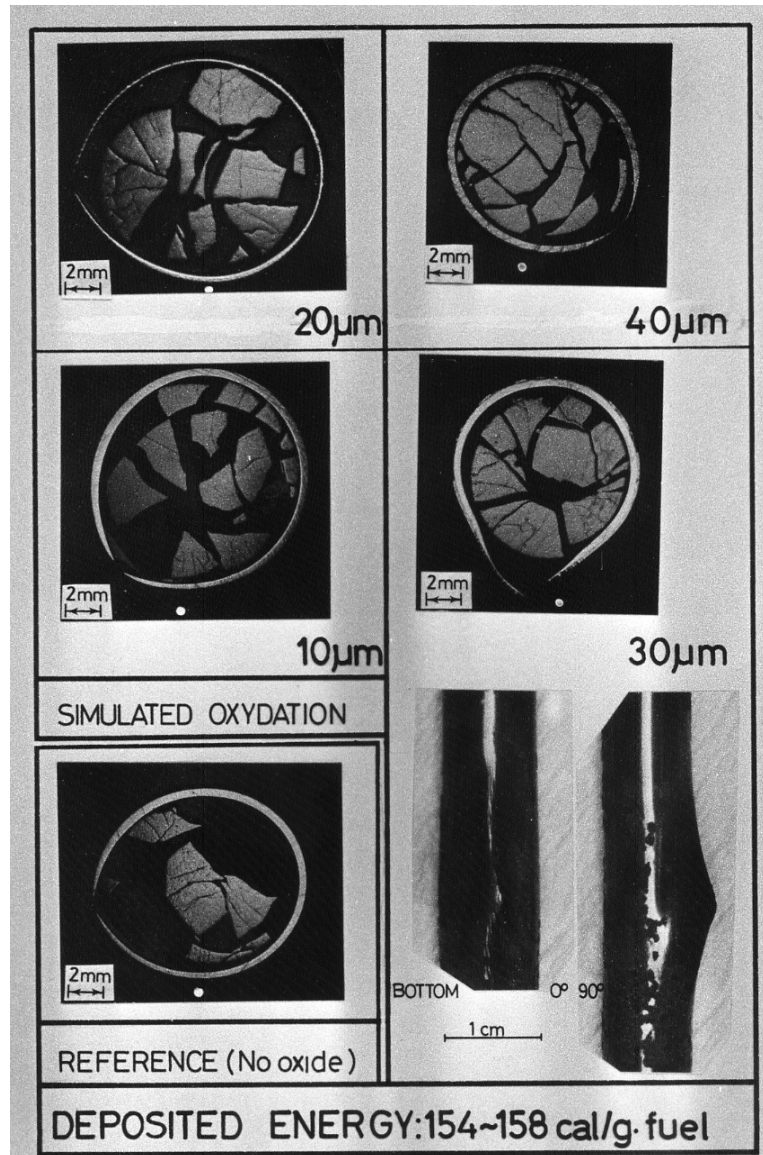

Photo.3 Overview of the failed fuel rods in the pressurized group, where they were exposed to the energy deposition level of 151-158 cal/g・fuel (enthalpies 121-125 cal/g・fuel); All fuels were pressurized to 3.3-3.5MPa with the gas composition of 95%He+1%Kr+4%Xe; White spots in each picture shows the zero orientation of the test fuel rod. Note that all fuel pellets after the ballooning were relocated during an unlading of the fuel rod from the irradiation capsule and during a necessary preparation prior to the cutting.

A number of the rupture point was only one in each defected fuel rod. With respect to the fuel rod with 30μm oxide film, ZrO_2 was partly scaled off and changed the original surface in spots (see, the picture). To understand the effect of ZrO_2 on the failure mechanism, the fuel rod with 30μm was examined in detail and the metallographic picture is shown in **Photo. 4**.
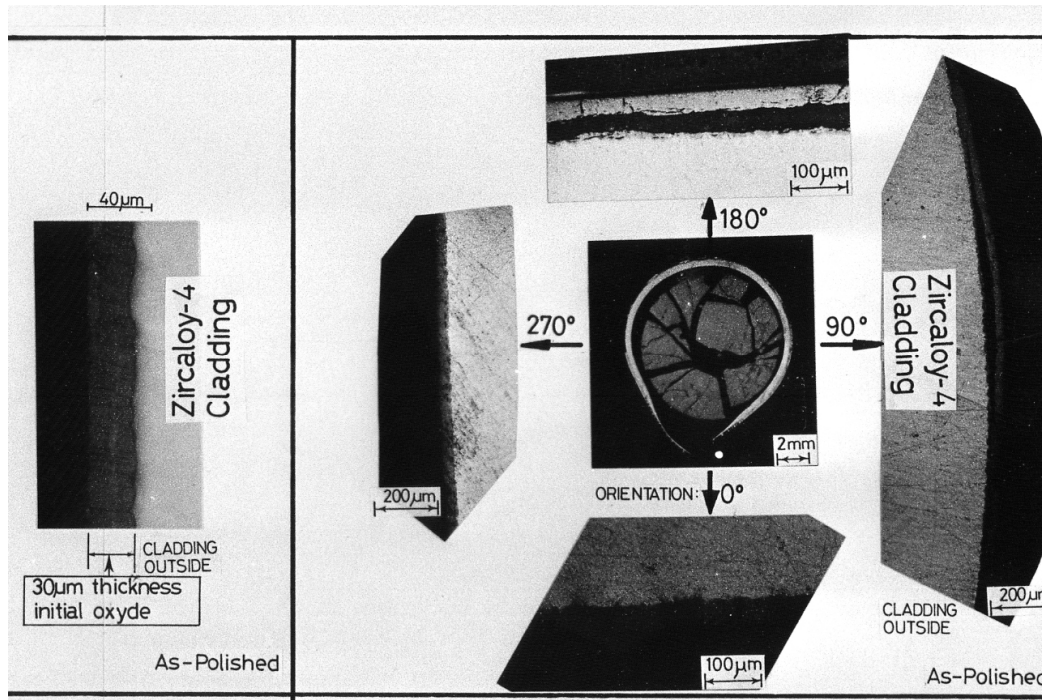
Photo.4 (Left) fabricated ZrO_2 dense and homogeneous oxide having a thickness of 30 μm. (Right) the cladding was ballooned and ruptured at the zero orientation (the photograph in the middle). The oxide film was scaled off (90 and 180 degree), chipped off (0 degree), and cracked (270 degree).

Taking into consideration that not only the standard fuels but also the ZrO_2 fuels were defected by the ballooning and rupture mechanism at the tested enthalpies, the author concluded within this experimental scope that for the case of pressurized PWR to 3.1-3.6MPa the influence of the ZrO_2 oxides on the failure mechanism was none.

3.1.2 Unpressurized group

For the case of the unpressurized fuels, the data plot was followed the example shown in the Licensing Guideline for RIA [12]. **Fig. 6** shows the result. While the failure of the waterside corroded (ZrO_2) fuels did not occur below the energy deposition of

260cal/g・fuel, all standard fuels failed at the energy depositions tested.
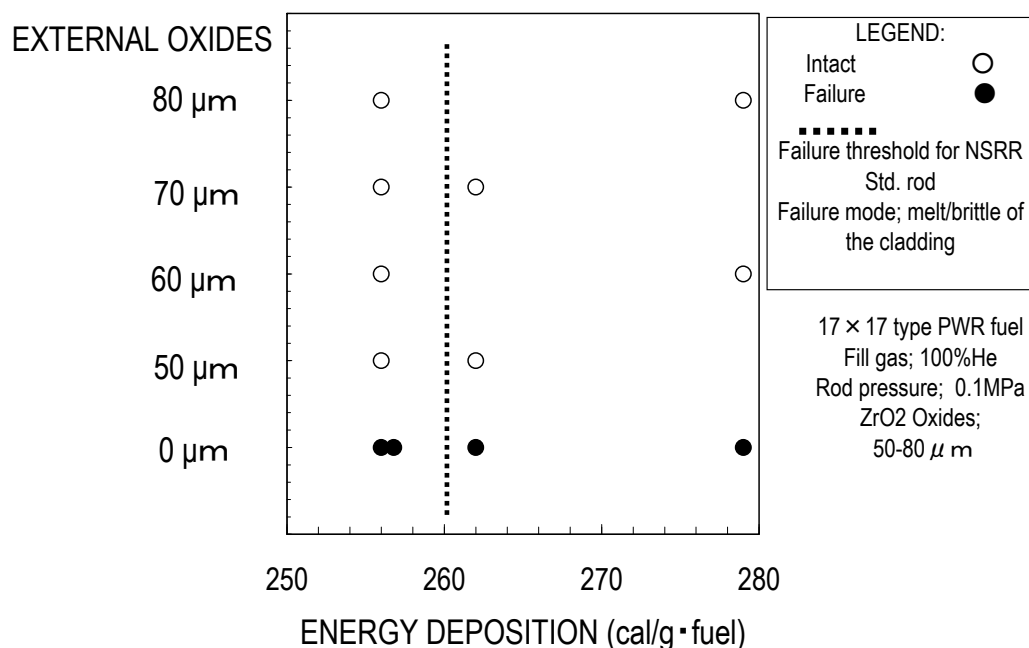

Fig.6   Failure and no failure of the unpressurized PWR fuels with experimental parameters.

Failure mechanism of this case was revealed by PIE. A typical overview of the waterside corroded fuel (J7, 80 μ m) and the reference one (J29, 0 μ m) is shown in the **Photo.5**, where the two fuels were pulsed at the energy deposition of 279 cal/g・fuel. It is clear from the picture that the former did not fail but the latter was broken into pieces at the rod bottom end and showed the wrinkle deformation overall cladding[1]. As indicated in the photograph, the author cut the two fuel rods at the half point of the active column length or mid T/C position for further detail metallographic study.

---

[1]   Due to the pulse a UO_2 pellet became a very hot and expanded promptly towards the cladding inside to cause PCMI. Because the interaction between the hot UO_2 and the cladding inside did not occur uniformly but occur at the local area, the cladding inside interacted was heated up and deformed causing a plastic flow of the cladding materials, that is, the cladding was melt in the area. As a result, the area was thinned due to the flow out and thermal tensile stress but the other area was thickened due to the material flow into that area. Lastly, the cladding thickness was partly thinned and partly thickened; the feature looked like a wrinkle. Therefore the author defined it as the wrinkle deformation. Of course this type of deformation accompanies the radial crack propagation mostly at the thinned area because the cladding becomes brittle and easy to have a tensile stress when it is quenched. Namely, the wrinkle deformation represents the cladding melt/brittle failure. This type of the failure is typical for the unpressurized fuel but not for pressurized fuel.
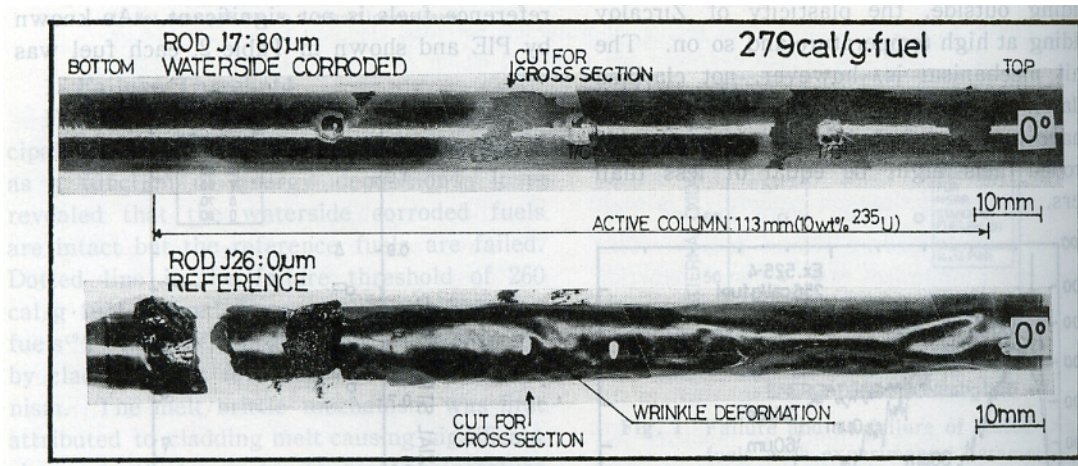
Photo.5 Overview of the waterside corroded fuel (rod J7, 80 μ mZrO$_2$, top) and the reference fuel (rod J26, 0 μ mZrO$_2$, bottom) at the energy deposition of 279cal/g・fuel.

Photo 6 is the resultant metallographic pictures. A recorded peak cladding surface temperature (PCST) for the waterside corroded fuel rod at the cut position was about 1,800 deg. C; the value was significantly closed to the melting point of the cladding. Even though such situation, the waterside corroded fuel kept the external surface tight and the cladding thickness unchanged. There was no trace that an additional oxide layer was formed. On the other hand, in the reference fuel, an uniform oxide ZrO$_2$ at the cladding external was additionally formed to the magnitude of 98 μ m Continuing to that layer, the oxygen stabilized α phase and prior β phases to the inside were existed. A porous oxide seen innermost area might be formed after the occurrence of melt/brittle failure, that is, a reaction occurred between the cladding inside opened to the coolant and the immersed coolant after failure .

This metallographic comparison by the two pictures implied a very important experimental fact within this experimental scope that the waterside corrosion had a role to prevent the unpressurized fuel from the melt/brittle failure. How did the corroded ZrO$_2$ film prevent the cladding from the melt and brittle failure? The author considered that from the thermal point the corroded film prevented a significant temperature gradient across the cladding thickness because of its low heat conductivity; it was likely to withstand the plastic flow of the molten cladding material. From the mechanical point the corroded film worked as the mechanical barrier, hence it prevented the additional formation of the oxide film and suppressed the magnitude of hoop stress raised during the quench. The detail discussion about these points will be a subject of the subsequent section.
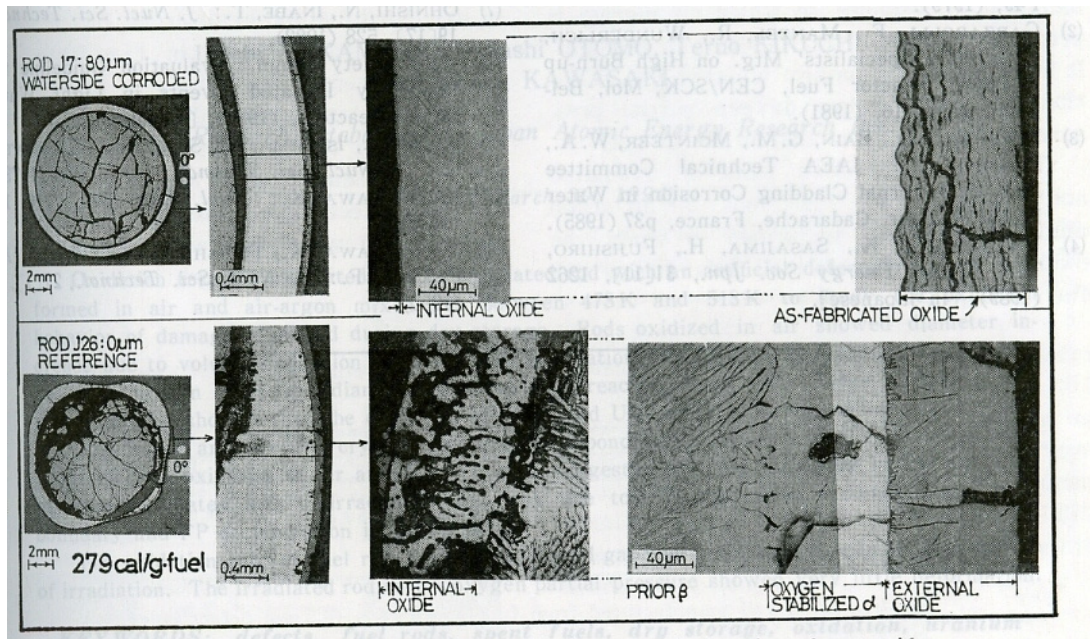
Photo.6 Cross sections cut from the mid T/C location of the waterside corroded fuel (rod J7, 80 μ mZrO$_2$, top) and the reference fuel (rod J26, 0 μ mZrO$_2$, bottom) at the energy deposition of 279cal/g・fuel.

3.2 Thermal and mechanical behavior

3.2.1 Thermal behavior

(1) PCST

(1-1) PCST

As shown in **Fig.7**, PCST of the pressurized group consisted of 6 data from the standard fuels and one data from the 40 μ m fuel (the rod no. P20). As a whole they did not exceed the 1,000 deg. C within this experimental scope. The effect of the waterside corrosion on PCST is not clear from the plotting and there is no significant difference in the behavior between the defected rod and intact rod.

PCST of the unpressurized group is, however, higher than that of pressurized group. Among unpressurized data, at the same energy deposition, the waterside corroded fuel showed lower temperature than that of the standard. For the reader's convenience, the author inserted two dotted lines for PCST, established by the past NSRR experiments for the standard fuels [24, 25]. Namely, the corroded film had a role to reduce the PCST significantly. In the figure, for example, PCST of the standard fuel was 1,748 deg. C (●), that of the 60 μ m fuel was 1,347 deg. C (□) and 80 μ m fuel was 1,285 deg. C

(＊) at 256cal/g・fuel. The maximum deviation was 463 (1748-1285) deg. C in this case, where the former was defected but the latter two were intact.
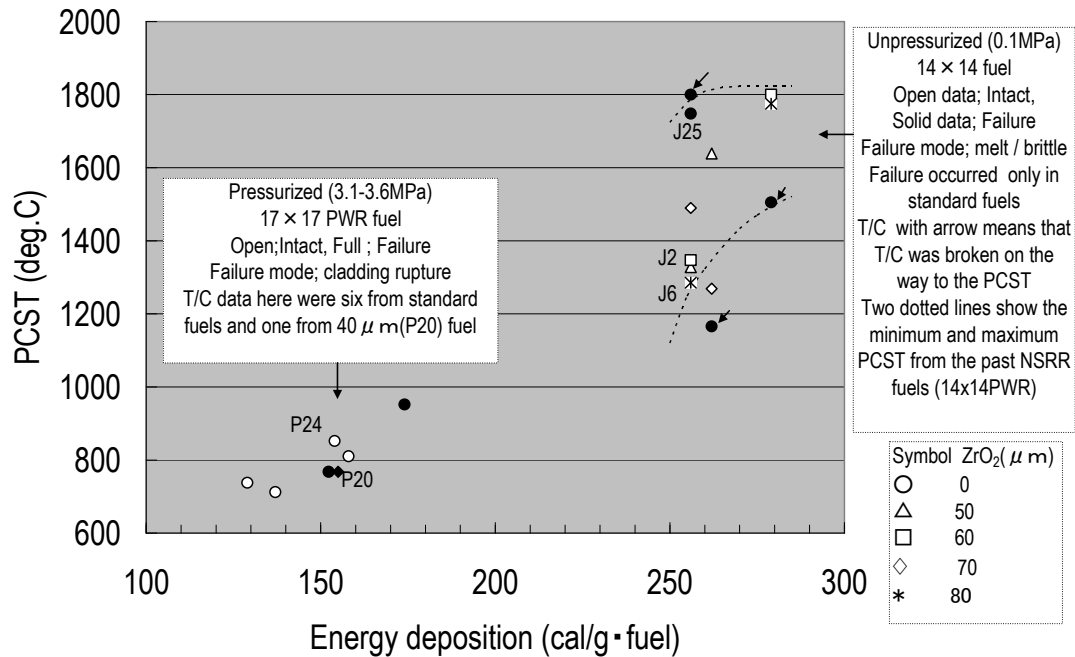

Fig.7 PCST vs. energy deposition for the pressurized group and the unpressurized one

(1-2) Cladding surface temperature

(1-2-1) Pressurized fuel

For the reader's convenience, the author prepared the cladding surface temperature (CST) data as shown in **Fig.8**. The data was obtained from experiment 524-4, where pressurized P24 (0 μ m), P18 (30 μ m) and P20 (40 μ m) were pulsed at 154 cal/g・fuel . Immediately after the pulse, three rods had the departure from the nucleate boiling (DNB)[2]. P24 and P20 had the PCST around 800deg. C as shown in Fig.7 but T/C data for P18 was malfunctive for only showing the PCST as high as 110 deg. C. Due to the extremely low PCST, the P18 was omitted from Fig.7.

(1-2-2) Unpressurized fuel

CST data for the unpressurized fuel is shown in **Fig. 9**. The data was obtained from experiment 525-4, where unpressurized J25 (0 μ m), J2 (60 μ m) and J6 (80 μ m) were

---

[2] The occurrence of DNB can be confirmed from the PIE because the DNB tended to burn the fuel rod surface and changed the color from silver gray to black along the active fuel column. Metallographic pictures shown in the Fig.8 were from PIE, showing that the three tested rods had DNB.

pulsed at 256 cal/g・fuel . As shown here, PCST of the standard fuel is higher than those of the waterside corroded fuels at the place of the mid T/C. However, The waterside corroded fuels caused the quenching faster than that of the standard fuel.
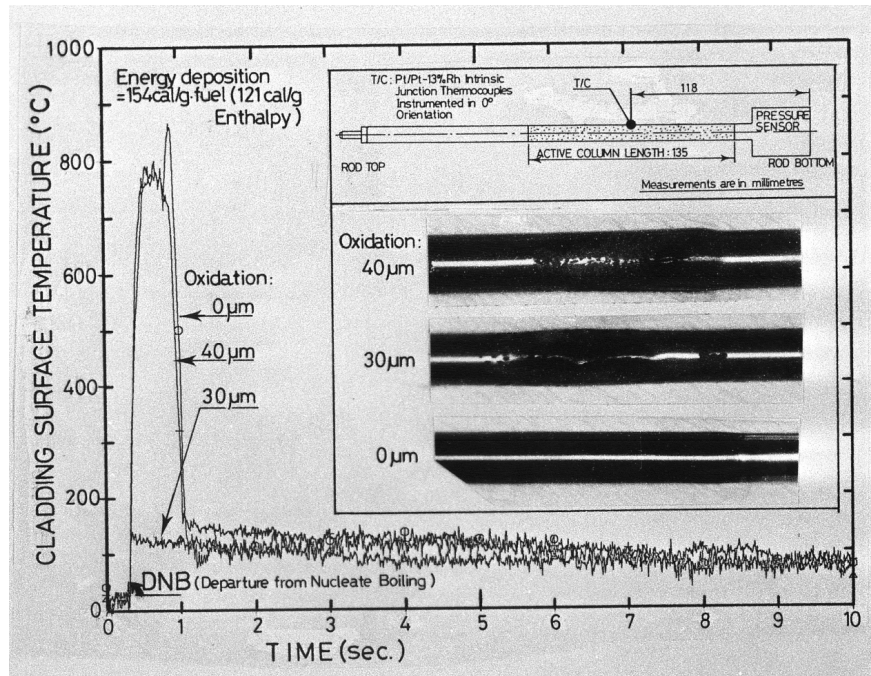

Fig. 8 Cladding surface temperature vs. time; three fuel rods of P24, P18 and P20 having 0, 30 and 40 μ m ZrO$_2$ film were provided. One T/C was as shown in the schematic figure and metallographic pictures spot welded at the zero orientation and mid point of the active fuel column. Two corroded fuels were ruptured but the standard one was intact.
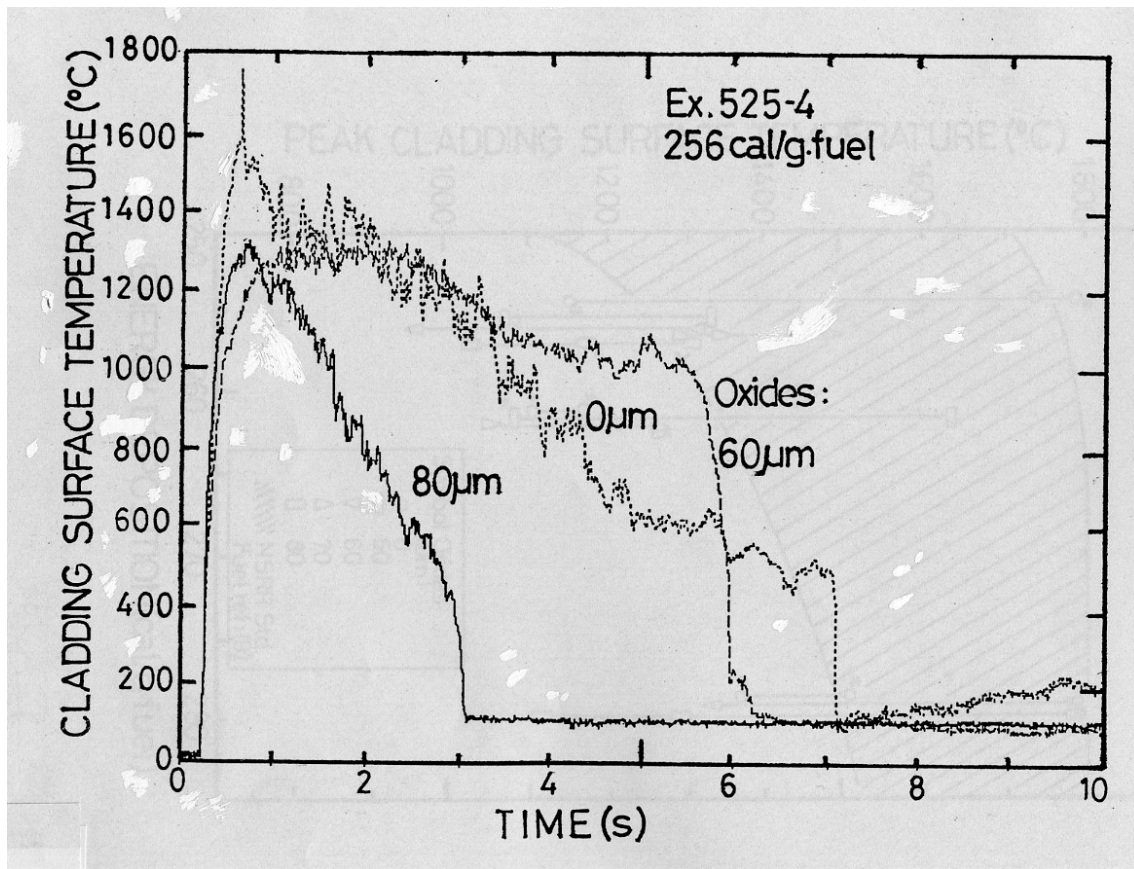
Fig. 9 Cladding surface temperature vs. time as a function of the oxide thickness; Data were from unpressurized fuels

(1-3) Accuracy of the PCST

A UO$_2$ fuel during the temperature transient should be relocated and moved randomly. As a natural consequence, T/C does not show the uniform temperature along the active fuel column. To understand this relocation effect on PCST, the author prepared three thermocouples and spot welded them at three different axial positions along zero deg. C generatrix. The mid T/C coincided with the middle of the active column length; bottom and top T/C were apart from ±33mm form the mid location. The fuel active length was divided into four pieces by the three thermocouples. As shown in **Fig.10**, three T/C data from axial different locations were obtained as a function of deposited energy; where mid T/C reading value was given by the full mark and others were top and bottom T/C reading value. It is clear from the figure that there occurred the fuel relocation and PCST at different location showed different reading points. It should be noted that the axial power profile at those T/C locations was flat, that is, a peaking factor was unity. During the present study, the author referred to the T/C at the mid position, which is

shown in the plotting as the full mark. Therefore the error band of PCST for the pressurized standard fuel was 9% for the worst case.
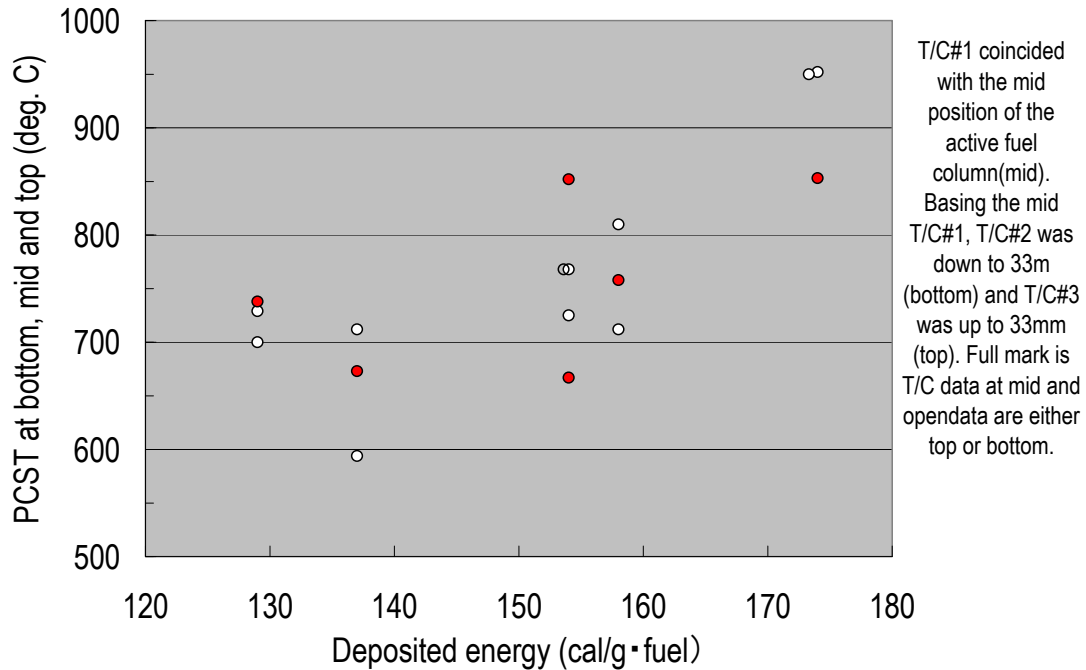

Fig.10 PCST read from the axially different locations (bottom, mid and top) as a function of the deposited energy; Data from the pressurized standard fuels

(2) Behavior at the quench

As shown in **Fig.11**, temperature drop ΔT as a function of time to quench tq is plotted[3]. ΔT for the pressurized fuel was below 800 deg. C and tq was less than 1s. However, ΔT for the unpressurized fuel is above 1,000 deg. C. and tq was larger than 1s. Because ΔT for the unpressurized fuel has a linear relationship to the tensile stress raised during the quench, a fuel with higher ΔT has a potential to cause the melt/brittle failure. As known from the plotting, the standard fuel at the highest ΔT was defected, however, all corroded fuels did not fail at all. A magnitude of ΔT was decreased as the use of the thicker corroded fuel, e.g., ΔT for the 80μ m rod is smaller than that of ΔT for the 50μ m rod.

For the corroded fuel, a time to quench tq was studied as shown in **Fig. 12**. It is interesting to say that with increase of the film thickness in the corroded fuel tq was

---

[3] Temperature drop ΔT is given by the PCST minus the temperature just after the quenching.
Time to quench tq is given by the time to PCST minus time to quench.

shortened. Namely, the use of the thicker ZrO_2 makes the fuel rod colder. For the pressurized fuel, tq is faster than that of unpressurized fuel.

To summed up, the author revealed that PCST, ΔT and tq for the corroded fuel are smaller than that of the standard fuel. These three factors are directly related to the melt/brittle mechanism, namely the low PSCT means that the UO_2 temperature is low, the small ΔT means that the thermal shock (tensile stress) during the quench is small and the short tq means that the interaction time between the hotter UO_2 and cladding is shortened. The author thinks that ZrO_2 film took a role of the thermal protector against the melt/brittle failure.
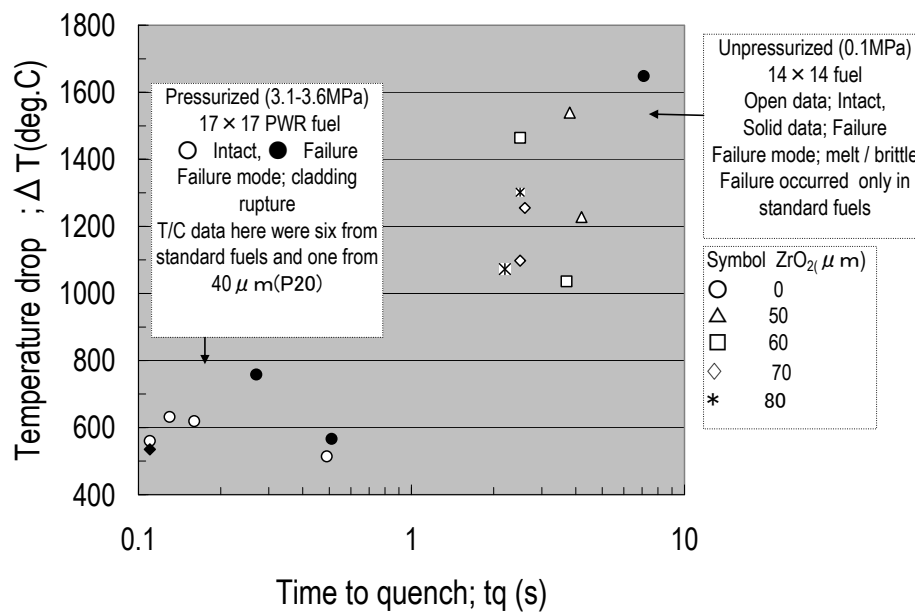
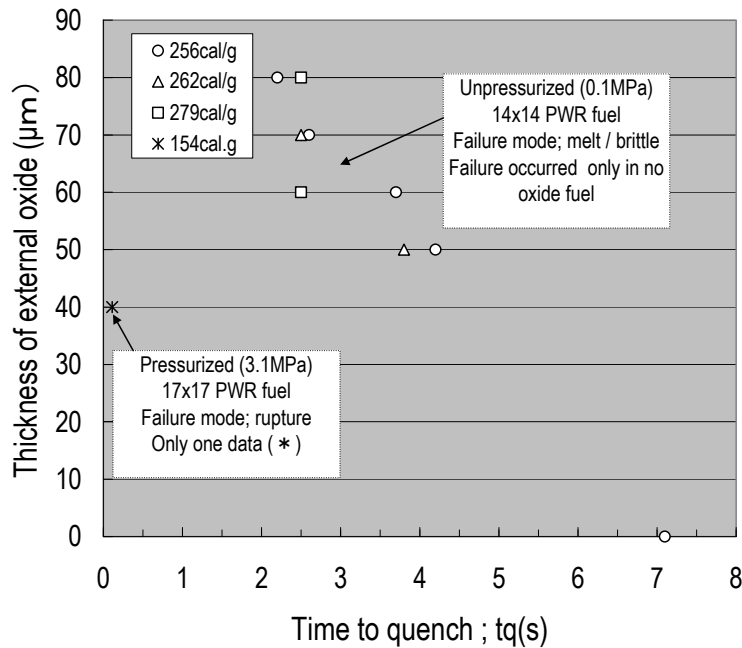Fig. 11 Temperature drop ΔT vs. time to quench

Fig.12 Thickness of waterside corroded fuel vs. time to quench tq

3.2.2 Mechanical Behavior

(1) Axial PCMI

(1-1) Axial PCMI

As shown in **Fig. 13**, a peak axial strain for the pressurized group was increased with the increase of the deposited energy. The maximum was 4%. As a tendency, the magnitude of the axial strain (ballooning) was bigger with the use of thicker ZrO_2. This might be because the ZrO_2 resisted to the rupture of the cladding at the outermost rim. A peak axial strain for the unpressurized group did not increase with the increase of the deposited energy and that of the ZrO_2 thickness. The value was almost the same level as much as 0.5-1.0%. This is because the strong axial restriction occurred by the closure of the radial gas gap immediately after the pulse. The peak axial strain for the unpressurized fuel was below 1% irrespective to the ZrO_2 oxides.
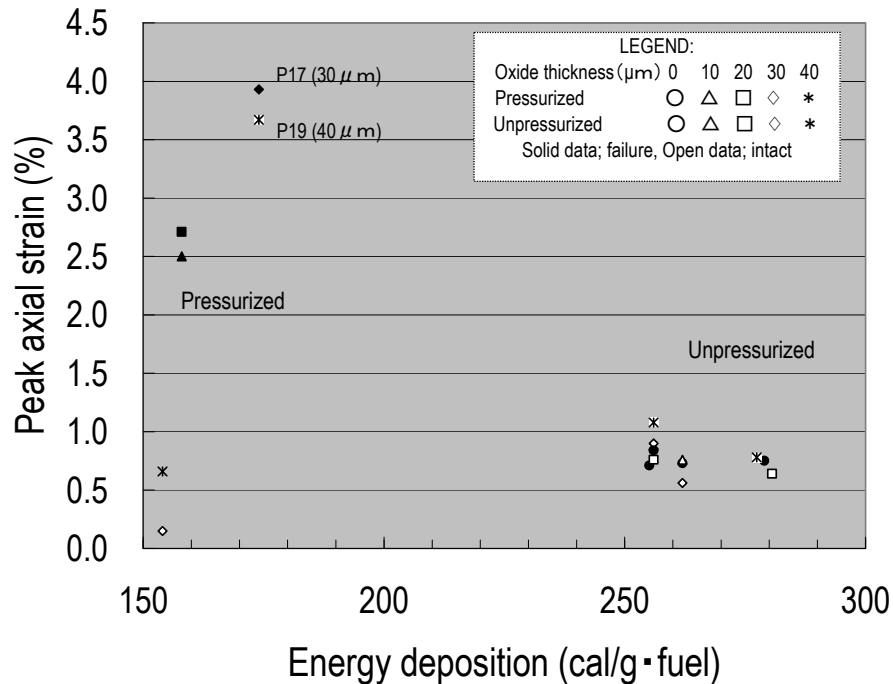
Fig.13 Peak axial strain vs. energy deposition for the standard fuels and the waterside corroded ones

(1-2) Time-dependent axial strain

For the reader's convenience, the author prepared the in-core axial strain data as shown in **Fig.14**. The data was obtained from experiment 524-3, where pressurized P9 (0 μ m), P17 (30 μ m) and P19 (40 μ m) were pulsed at 174 cal/g・fuel (142 cal/g・fuel in enthalpy). Because P9 had no EC, it was omitted from the plotting. Immediately after the pulse, axial strain of the two was increased and as shown in the Fig.11 they reached to the peak axial strain of 3.93% for P17 and 3.67% for P19. The magnitude was about 4 times the normal LWR fuel [15].

After reaching the peak, within 1s, the axial strain of P17 was suddenly dropped about 0.5% prior to starting the gradual decrease. The author would like to mention that Japanese fuel researchers called the phenomenon as the Onchi effect. The time coincided well with the time for the fuel failure, that is, a propagation of the cladding crack. The details on the Onchi effect are described elsewhere [16, 17]. Note that the axial strain of P19 did not show the Onchi effect and decreased its magnitude gradually. At 10s, the two data were reached to the same level together. This is the typical pattern

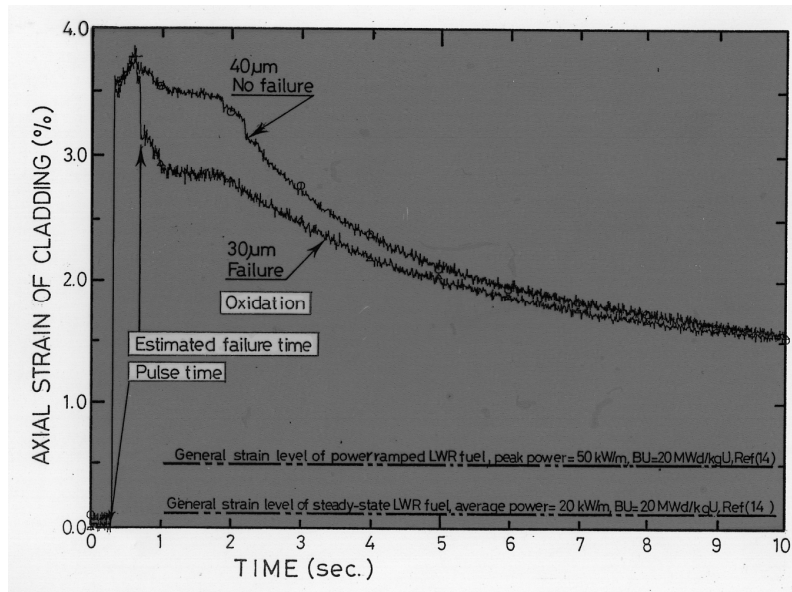known as the elastic-plastic deformation.

Fig.14 Axial strain of the corroded cladding vs. time; Two dotted lines are general axial strain levels of LWR fuels at steady-state operation (20kW/m) and at power ramp condition (50kW/m) [15].

As shown in **Fig. 15**, from the viewpoint of the rod internal pressure, the author made observation to the same rod group used in experiment 524-3. At that time, P9 (0μm) had the PF sensor, so that the rod internal pressures of the three rods were able to monitor. It is worthy of mentioning that 05s after the pulse P9 (0μm) and P17 (30μm) have lost their pressures. Their data had the same pressure as that of the coolant after 1.8s. The time to rupture observed from the pressure data (0.5s) coincided with that observed from the Onchi effect (0.5s).
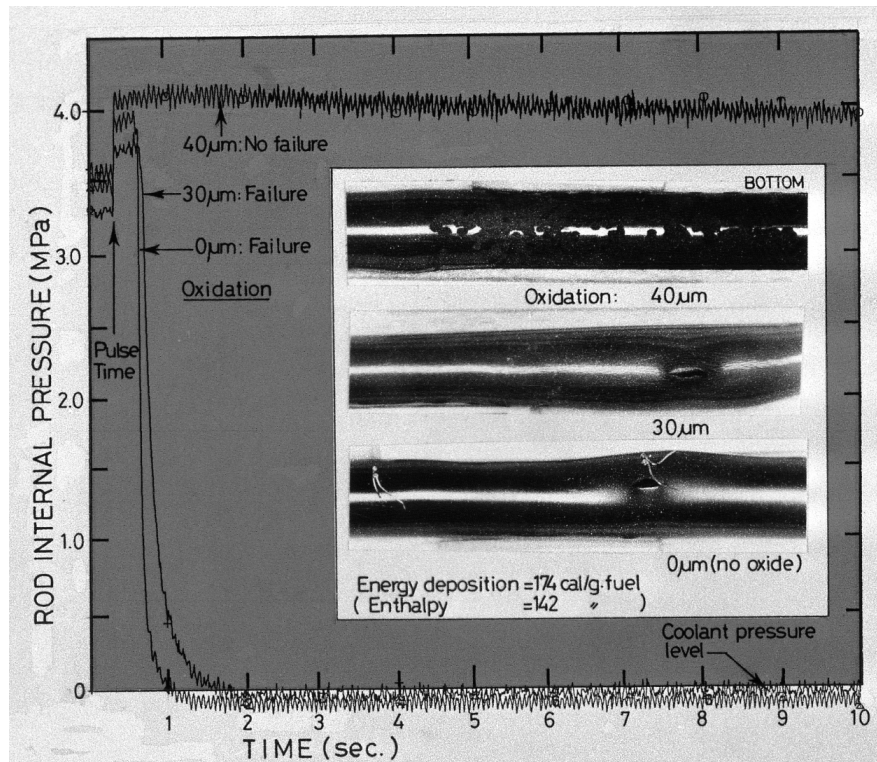
Fig.15 Change of the rod internal pressure vs. time as a function of ZrO_2 thickness; A rod overview obtained from PIE was included.

(1-3) Accuracy of the axial strain

In the case of the pressurized fuel, the author used the movement marker to verify the axial strain data monitored by the strain gauge type pressure sensor. The result of the verification is shown in **Fig. 16.** Because the movement marker was set on the top of fuel column, the maximum moved distance should be equal to the axial peak strain. In practical, however, one case showed a good agreement but the other case showed not. The reading value from the movement marker was tended to overestimated (400%) at the 154 cal/g・fuel and underestimated (30%) at 158 and 174 cal/g・fuel. The relative good accuracy in the latter case was due to the occurrence of the gap closure, where the fuel column moved together with the cladding under the action of the strong PCMI.
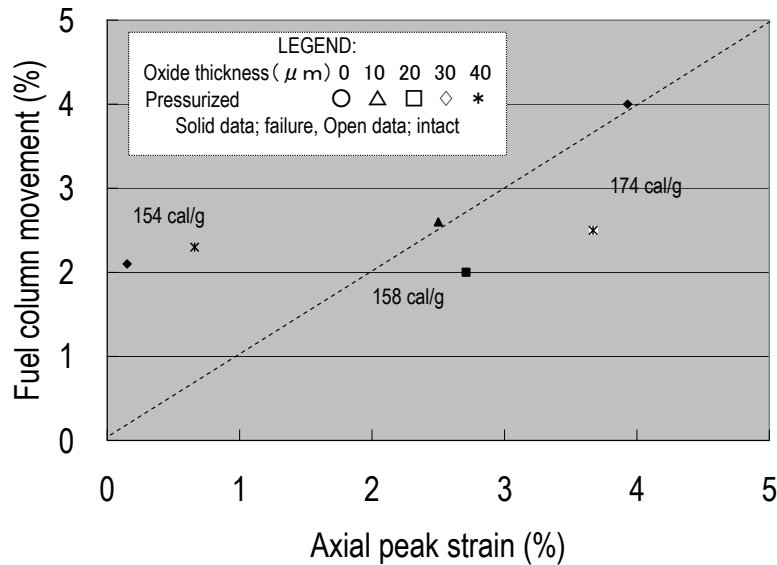
Fig. 16 Fuel column movement vs. Axial peak strain obtained from the pressurized fuels

(2) Radial PCMI

As shown in **Fig.17**, the residual diametral strain[4] for the pressurized fuel ranged from 2% to 10%, which was bigger than that of peak axial strain due to the ballooning. On the other hand, the residual diametral strain for the unpressurized fuel ranged below 4%, which was equal or bigger than that of the peak axial strain because of the strong radial PCMI. For the pressurized group, as the genera tendency, the magnitude of the residued diametral strain in the corroded fuels was smaller than that in the standard fuels. The effect of ZrO_2 on failure is not clear. For example, P19 (40 μ m, no failure) in the plotting had a peak axial strain by 3.7% but the residual diametral strain was about 3%. P20 (40 μ m, failure) had a peak axial strain by 0.66% but the residual diametral strain was 3.6%.

For the unpressurized group, the magnitude of the residual diametral strain in the corroded fuels is smaller than that in the standard fuels. Namely, not only in the pressurized fuels but also in the unpressurized fuels, ZrO_2 could suppress the residual diametral strain at the outermost rim.

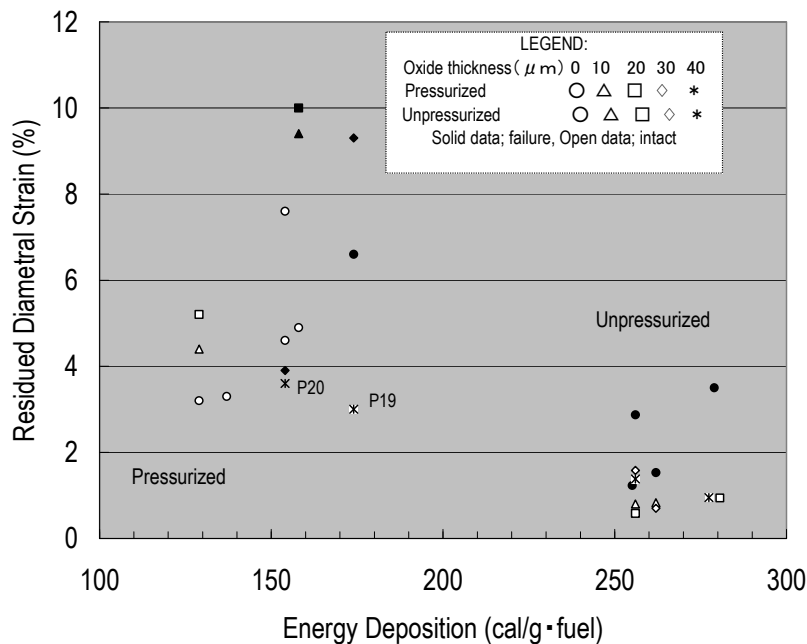
[4] A rod averaged value including the rupture position.

Fig.17 Residual diametral strain vs. energy deposition for the standard fuels and the
waterside corroded ones

3.2.3 PIE

(1) Bow

PIE was performed in detail for the unpressurized fuels. All test rods were bowed by the
magnitude from 1mm to 9mm, as shown in the previous Table 4-2.

(2) Grain growth

Irrespective to the waterside corrosion, a grain growth of the UO$_2$ fuel at the fuel
periphery occurred. The original grain size by 10μm was increased to 36μm for the
corroded fuel J1 (50μm ZrO$_2$, PCST was 1,539deg.C) and 90μm for the standard
fuel J26(0μm ZrO$_2$, PCST was unknown). The grain growth was a very local
phenomenon having the width about 0.3mm. The mechanism of this phenomenon was
described elsewhere [18].

(3) DNB and Oxidation of the cladding outside

The author should be said that the waterside corroded fuel did not form additional ZrO$_2$
film during and after the pulse irradiation. However, the standard fuel after DNB formed
the ZrO$_2$ film at the cladding outside sized by about $86\pm14\mu$m from the energy
deposition of 256cal/g・fuel. This was happened in parallel to the cladding melt and
brittle process. The author understands that the oxides become brittle during quench and
occasionally caused the through-wall cracking. The additional effects were not revealed.

4. CONCLUSIONS

For the PWR fuel under the power transient, an influence of the waterside corrosion up to 80μ m on the failure threshold and its mechanism was studied taking into consideration of the rod internal pressure as a variable. Obtained results are as follows:

- For the pressurized PWR fuels up to 3.1-3.6MPa, the waterside corrosion had no effect on the fuel failure mechanism occurred by the ballooning/rupture. The failure threshold of those was the same as that observed in the standard fuel. For the unpressurized PWR fuels, the waterside corrosion had a significant effect to prevent them from the failure, occurred by the melt/brittle mechanism. The ZrO_2 film contributed to minimize the temperature gradient across the cladding, prevent the formation of the additional oxide and restrain the hoop stress raised during the quench. The failure threshold of the corroded fuels was higher than that of the standard fuel.

- The use of the ZrO_2 film in the unpressurized fuels suppressed the magnitude of PCST, ΔT and shortened the time to quench. For example, PCST was 1,748 deg. C for the standard fuel but 1,285 deg. C for the corroded fuel (80μ m) at the energy deposition of 256cal/g・fuel. The PCST as much as 463 deg. C was suppressed.

- For the axial PCMI, the peak axial strain for the pressurized fuel increased with the increase of ZrO_2 film; the maximum was 4% for the 40μ m. At the outermost rim ZrO_2 film suppressed the cladding to balloon. By contrast, the axial PCMI for the unpressurized fuel was less than 1%, irrespective to the ZrO_2 film. This was duel to the rapid gap closure by the swelled hot fuel. For the radial PCMI, the ZrO_2 film suppressed the residual diametral strain, irrespective to the pressurization.

- The error band of the PCST in the pressurized fuels was 9% in maximum and that of the axial peak strain estimated by the movement marker was ranged from 400% to 30%. Time to failure for the ruptured PWR fuel was within 1s.

REFERENCES

[1]   Garzarolli, F., Stehle, H.: IAEA. Int. Symposium on Improvement on Water Reactor Fuel Technology and Utilization, Stockholm, Sweden, (1986).

[2]   Tulenko, T. S., *et al.*: ANS Topical Meeting on Light Water Reactor Fuel Performance, Portland, Oregon, USA, (1979).

[3]   Andrews, M. G., *et al.*: ANS Topical Meeting on Light Water Reactor Performance, Williamsburg, Virginia, USA, (1988).

[4]   Balfour, M. G., *et al.*: *WCAP*-10180, (1982).

[5]   Dyecha, T. D., *et al.*: IAEA Technical Committee Meeting on External Corrosion in Water Power Reactor, Cadarache, France, (1985).

[6]   Reshetnikov, F. G., *et al.*: ibid.

[7]   Suzuki, S., *et al.* : Ref.(1).

[8]   Irisa, Y., *et al.* : Ref.(3).

[9]   Garzarolli, F., *et al.*: IAEA Specialists' Meeting on High Burnup in Power Reactor Fuel, CEN/SCK, Mol, Belgium, (1981).

[10]   Garzarolli, F., *et al.*: ANS Topical Meeting on Light Water Reactor Fuel Performance, Orlando, Florida, USA, (1985).

[11]   Coleman, T. A., *et al.*: ANS Topical Meeting on LWR External Burnup –Fuel Performance and Utilization, Williamsburg, Virginia, (1985).

[12]   The Nuclear Safety Commission of Japan; Evaluating Reactivity Insertion Events of Light Water Nuclear Power Reactor Facilities, Regulatory Guide *L-SE-I* 03 (1984.1).

[13]   *ASTM-E* 321-79, (1985).

[14]   Ohnishi, N., Inabe, T.: *J. Nuclear Science and Technology*, **19** [7], 528 (1982).

[15]   Yanagisawa, K., Kondo, Y., and Kolstad, E.: *J. At. Energy Soc. Japan,* **28**[7], 641 (1986).

[16]   Yanagisawa, K., Devold, H.: *J. At. Energy Soc. Japan,* **28**[8], 771 (1986).

[17]   Ichikawa, M et al; ANS Topical Meeting on Light Water Reactor Performance, Williamsburg, Virginia, USA, (1988).

[18]   Yanagisawa, K.: Failure Mechanism of Nb_2O_5 Doped PWR Fuels under Power Transient, *JAEA-Review* 2010-054 (2010).

[19]   Saito, S., Ishijima, K., Shiozawa, S., Iwata, K.: *J. Nucl. Sci. Technol.*, **14** [3], 226 (1973).

[20]   Yanagisawa, K.: Transient Behavior of Water side Corroded PWR fuel, *J. Nucl. Sci. Technol.*, **32** [4], 313 (1995).

[21]   Yanagisawa, K., Sasajima, H., Fujishiro, T: Behavior of PWR Fuels during

Reactivity Initiated Accident Conditions, (I) Influence of Waterside Corrosion, *J. At. Energy Soc. Japan,* **31** [11], 1262(1989).

[22]   Reactivity Accident Laboratory and NSRR Operation Division: Annual Progress Report on the NSRR Experiments (21) (April 1989 through March 1990), *JAERI-M* 92-072, (1992). <in Japanese>

[23]   Yanagisawa, K.: Influence of Waterside Corrosion, Proc., the 12th NSRR and Severe Accident Technical Review Meeting, Nov. 8 to 10, (1988).

[24]   Yanagisawa, K.: *Nucl. Eng. Des.,* **116**, 171 (1989).

[25]   Yanagisawa, K., Fujishiro, T., Negrini, A., Franco, F: *J. Nucl. Sci. Technol.*, **27** [1], 56 (1990).

国際単位系（SI）

表1．SI基本単位

基本量	SI基本単位 名称	記号
長　　さ	メートル	m
質　　量	キログラム	kg
時　　間	秒	s
電　　流	アンペア	A
熱力学温度	ケルビン	K
物　質　量	モル	mol
光　　度	カンデラ	cd

表2．基本単位を用いて表されるSI組立単位の例

組立量	SI基本単位 名称	記号
面　　　　　積	平方メートル	m^2
体　　　　　積	立法メートル	m^3
速さ，速　度	メートル毎秒	m/s
加　速　度	メートル毎秒毎秒	m/s^2
波　　　　　数	毎メートル	m^{-1}
密度，質量密度	キログラム毎立方メートル	kg/m^3
面　積　密　度	キログラム毎平方メートル	kg/m^2
比　　体　　積	立方メートル毎キログラム	m^3/kg
電　流　密　度	アンペア毎平方メートル	A/m^2
磁界の強さ	アンペア毎メートル	A/m
量濃度(a)，濃度	モル毎立方メートル	mol/m^3
質　量　濃　度	キログラム毎立法メートル	kg/m^3
輝　　　　　度	カンデラ毎平方メートル	cd/m^2
屈　折　率(b)	（数字の）1	1
比　透　磁　率(b)	（数字の）1	1

(a) 量濃度（amount concentration）は臨床化学の分野では物質濃度（substance concentration）ともよばれる。
(b) これらは無次元量あるいは次元1をもつ量であるが、そのことを表す単位記号である数字の1は通常は表記しない。

表5．SI接頭語

乗数	接頭語	記号	乗数	接頭語	記号
10^{24}	ヨ　タ	Y	10^{-1}	デ　シ	d
10^{21}	ゼ　タ	Z	10^{-2}	センチ	c
10^{18}	エクサ	E	10^{-3}	ミ　リ	m
10^{15}	ペ　タ	P	10^{-6}	マイクロ	µ
10^{12}	テ　ラ	T	10^{-9}	ナ　ノ	n
10^{9}	ギ　ガ	G	10^{-12}	ピ　コ	p
10^{6}	メ　ガ	M	10^{-15}	フェムト	f
10^{3}	キ　ロ	k	10^{-18}	ア　ト	a
10^{2}	ヘクト	h	10^{-21}	ゼプト	z
10^{1}	デ　カ	da	10^{-24}	ヨクト	y

表6．SIに属さないが、SIと併用される単位

名称	記号	SI単位による値
分	min	1 min=60s
時	h	1h =60 min=3600 s
日	d	1 d=24 h=86 400 s
度	°	1°=(π/180) rad
分	'	1'=(1/60)°=(π/10800) rad
秒	"	1"=(1/60)'=(π/648000) rad
ヘクタール	ha	$1ha=1hm^2=10^4m^2$
リットル	L, l	$1L=1l=1dm^3=10^3cm^3=10^{-3}m^3$
トン	t	$1t=10^3$ kg

表3．固有の名称と記号で表されるSI組立単位

組立量	SI組立単位 名称	記号	他のSI単位による表し方	SI基本単位による表し方
平　面　角	ラジアン(b)	rad	1 (b)	m/m
立　体　角	ステラジアン(b)	sr(c)	1 (b)	m^2/m^2
周　波　数	ヘルツ(d)	Hz		s^{-1}
力	ニュートン	N		$m\ kg\ s^{-2}$
圧力，応力	パスカル	Pa	N/m^2	$m^{-1}\ kg\ s^{-2}$
エネルギー，仕事，熱量	ジュール	J	N m	$m^2\ kg\ s^{-2}$
仕事率，工率，放射束	ワット	W	J/s	$m^2\ kg\ s^{-3}$
電荷，電気量	クーロン	C		s A
電位差（電圧），起電力	ボルト	V	W/A	$m^2\ kg\ s^{-3}\ A^{-1}$
静　電　容　量	ファラド	F	C/V	$m^{-2}\ kg^{-1}\ s^4\ A^2$
電　気　抵　抗	オーム	Ω	V/A	$m^2\ kg\ s^{-3}\ A^{-2}$
コンダクタンス	ジーメンス	S	A/V	$m^{-2}\ kg^{-1}\ s^3\ A^2$
磁　束	ウェーバ	Wb	Vs	$m^2\ kg\ s^{-2}\ A^{-1}$
磁　束　密　度	テスラ	T	Wb/m^2	$kg\ s^{-2}\ A^{-1}$
インダクタンス	ヘンリー	H	Wb/A	$m^2\ kg\ s^{-2}\ A^{-2}$
セルシウス温度	セルシウス度(e)	℃		K
光　　束	ルーメン	lm	cd sr(c)	cd
照　　度	ルクス	lx	lm/m^2	$m^{-2}\ cd$
放射性核種の放射能(f)	ベクレル(d)	Bq		s^{-1}
吸収線量，比エネルギー分与，カーマ	グレイ	Gy	J/kg	$m^2\ s^{-2}$
線量当量，周辺線量当量，方向性線量当量，個人線量当量	シーベルト(g)	Sv	J/kg	$m^2\ s^{-2}$
酸　素　活　性	カタール	kat		$s^{-1}\ mol$

(a)SI接頭語は固有の名称と記号を持つ組立単位と組み合わせても使用できる。しかし接頭語を付した単位はもはやコヒーレントではない。
(b)ラジアンとステラジアンは数字の1に対する単位の特別な名称で、量についての情報をつたえるために使われる。実際には、使用する時には記号rad及びsrが用いられるが、習慣として組立単位としての記号である数字の1は明示されない。
(c)測光学ではステラジアンという名称と記号srを単位の表し方の中に、そのまま維持している。
(d)ヘルツは周期現象についてのみ、ベクレルは放射性核種の統計的過程についてのみ使用される。
(e)セルシウス度はケルビンの特別な名称で、セルシウス温度を表すために使用される。セルシウス度とケルビンの単位の大きさは同一である。したがって、温度差や温度間隔を表す数値はどちらの単位で表しても同じである。
(f)放射性核種の放射能（activity referred to a radionuclide）は、しばしば誤った用語で"radioactivity"と記される。
(g)単位シーベルト（PV,2002,70,205）についてはCIPM勧告2（CI-2002）を参照。

表7．SIに属さないが、SIと併用される単位で、SI単位で表される数値が実験的に得られるもの

名称	記号	SI単位で表される数値
電子ボルト	eV	$1eV=1.602\ 176\ 53(14)×10^{-19}J$
ダルトン	Da	$1Da=1.660\ 538\ 86(28)×10^{-27}kg$
統一原子質量単位	u	1u=1 Da
天文単位	ua	$1ua=1.495\ 978\ 706\ 91(6)×10^{11}m$

表8．SIに属さないが、SIと併用されるその他の単位

名称	記号	SI単位で表される数値
バール	bar	$1\ bar=0.1MPa=100kPa=10^5Pa$
水銀柱ミリメートル	mmHg	1mmHg=133.322Pa
オングストローム	Å	$1\ Å=0.1nm=100pm=10^{-10}m$
海里	M	1 M=1852m
バーン	b	$1\ b=100fm^2=(10^{-12}cm)2=10^{-28}m^2$
ノット	kn	1 kn=(1852/3600)m/s
ネーパ	Np	SI単位との数値的な関係は、対数量の定義に依存。
ベル	B	
デジベル	dB	

表4．単位の中に固有の名称と記号を含むSI組立単位の例

組立量	SI組立単位 名称	記号	SI基本単位による表し方
粘　　度	パスカル秒	Pa s	$m^{-1}\ kg\ s^{-1}$
力のモーメント	ニュートンメートル	N m	$m^2\ kg\ s^{-2}$
表　面　張　力	ニュートン毎メートル	N/m	$kg\ s^{-2}$
角　速　度	ラジアン毎秒	rad/s	$m\ m^{-1}\ s^{-1}=s^{-1}$
角　加　速　度	ラジアン毎秒毎秒	rad/s^2	$m\ m^{-1}\ s^{-2}=s^{-2}$
熱流密度，放射照度	ワット毎平方メートル	W/m^2	$kg\ s^{-3}$
熱容量，エントロピー	ジュール毎ケルビン	J/K	$m^2\ kg\ s^{-2}\ K^{-1}$
比熱容量，比エントロピー	ジュール毎キログラム毎ケルビン	J/(kg K)	$m^2\ s^{-2}\ K^{-1}$
比エネルギー	ジュール毎キログラム	J/kg	$m^2\ s^{-2}$
熱　伝　導　率	ワット毎メートル毎ケルビン	W/(m K)	$m\ kg\ s^{-3}\ K^{-1}$
体積エネルギー	ジュール毎立方メートル	J/m^3	$m^{-1}\ kg\ s^{-2}$
電　界　の　強　さ	ボルト毎メートル	V/m	$m\ kg\ s^{-3}\ A^{-1}$
電　荷　密　度	クーロン毎立方メートル	C/m^3	$m^{-3}\ sA$
表　面　電　荷	クーロン毎平方メートル	C/m^2	$m^{-2}\ sA$
電束密度，電気変位	クーロン毎平方メートル	C/m^2	$m^{-2}\ sA$
誘　電　率	ファラド毎メートル	F/m	$m^{-3}\ kg^{-1}\ s^4\ A^2$
透　磁　率	ヘンリー毎メートル	H/m	$m\ kg\ s^{-2}\ A^{-2}$
モルエネルギー	ジュール毎モル	J/mol	$m^2\ kg\ s^{-2}\ mol^{-1}$
モルエントロピー，モル熱容量	ジュール毎モル毎ケルビン	J/(mol K)	$m^2\ kg\ s^{-2}\ K^{-1}\ mol^{-1}$
照射線量（X線及びγ線）	クーロン毎キログラム	C/kg	$kg^{-1}\ sA$
吸　収　線　量　率	グレイ毎秒	Gy/s	$m^2\ s^{-3}$
放　射　強　度	ワット毎ステラジアン	W/sr	$m^4\ m^{-2}\ kg\ s^{-3}=m^2\ kg\ s^{-3}$
放　射　輝　度	ワット毎平方メートル毎ステラジアン	$W/(m^2\ sr)$	$m^2\ m^{-2}\ kg\ s^{-3}=kg\ s^{-3}$
酵　素　活　性　濃　度	カタール毎立方メートル	kat/m^3	$m^{-3}\ s^{-1}\ mol$

表9．固有の名称をもつCGS組立単位

名称	記号	SI単位で表される数値
エルグ	erg	$1\ erg=10^{-7}\ J$
ダイン	dyn	$1\ dyn=10^{-5}N$
ポアズ	P	$1\ P=1\ dyn\ s\ cm^{-2}=0.1Pa\ s$
ストークス	St	$1\ St=1cm^2\ s^{-1}=10^{-4}m^2\ s^{-1}$
スチルブ	sb	$1\ sb=1cd\ cm^{-2}=10^4cd\ m^{-2}$
フォト	ph	$1\ ph=1cd\ sr\ cm^{-2}\ 10^4lx$
ガル	Gal	$1\ Gal=1cm\ s^{-2}=10^{-2}ms^{-2}$
マクスウェル	Mx	$1\ Mx=1G\ cm^2=10^{-8}Wb$
ガウス	G	$1\ G=1Mx\ cm^{-2}=10^{-4}T$
エルステッド(c)	Oe	$1\ Oe ≙ (10^3/4π)A\ m^{-1}$

(c) 3元系のCGS単位系とSIでは直接比較できないため、等号「 ≙ 」は対応関係を示すものである。

表10．SIに属さないその他の単位の例

名称	記号	SI単位で表される数値
キュリー	Ci	$1\ Ci=3.7×10^{10}Bq$
レントゲン	R	$1\ R=2.58×10^{-4}C/kg$
ラド	rad	$1\ rad=1cGy=10^{-2}Gy$
レム	rem	$1\ rem=1\ cSv=10^{-2}Sv$
ガンマ	γ	$1\ γ=1\ nT=10^{-9}T$
フェルミ		$1フェルミ=1\ fm=10^{-15}m$
メートル系カラット		$1メートル系カラット=200\ mg=2×10^{-4}kg$
トル	Torr	$1\ Torr=(101\ 325/760)\ Pa$
標準大気圧	atm	1 atm = 101 325 Pa
カロリー	cal	1cal=4.1858J（「15℃」カロリー），4.1868J（「IT」カロリー）4.184J（「熱化学」カロリー）
ミクロン	µ	$1\ µ=1µm=10^{-6}m$